Plasma membrane aminoglycerolipid flippase function is required for signaling competence in the yeast mating pheromone response pathway

Elodie Sartorel, Evelyne Barrey*, Rebecca K. Lau†, and Jeremy Thorner
Division of Biochemistry, Biophysics and Structural Biology, Department of Molecular and Cell Biology, University of California, Berkeley, Berkeley, CA 94720-3202

ABSTRACT **The class 4 P-type ATPases ("flippases") maintain membrane asymmetry by translocating phosphatidylethanolamine and phosphatidylserine from the outer leaflet to the cytosolic leaflet of the plasma membrane. In *Saccharomyces cerevisiae*, five related gene products (Dnf1, Dnf2, Dnf3, Drs2, and Neo1) are implicated in flipping of phosphatidylethanolamine, phosphatidylserine, and phosphatidylcholine. In *MAT*a cells responding to α-factor, we found that Dnf1, Dnf2, and Dnf3, as well as the flippase-activating protein kinase Fpk1, localize at the projection ("shmoo") tip where polarized growth is occurring and where Ste5 (the central scaffold protein of the pheromone-initiated MAPK cascade) is recruited. Although viable, a *MAT*a *dnf1Δ dnf2Δ dnf3Δ* triple mutant exhibited a marked decrease in its ability to respond to α-factor, which we could attribute to pronounced reduction in Ste5 stability resulting from an elevated rate of its Cln2·Cdc28-initiated degradation. Similarly, a *MAT*a *dnf1Δ dnf3Δ drs2Δ* triple mutant also displayed marked reduction in its ability to respond to α-factor, which we could attribute to inefficient recruitment of Ste5 to the plasma membrane due to severe mislocalization of the cellular phosphatidylinositol 4-phosphate and phosphatidylinositol 4,5-*bis*phosphate pools. Thus proper remodeling of plasma membrane aminoglycerolipids and phosphoinositides is necessary for efficient recruitment, stability, and function of the pheromone signaling apparatus.**

Monitoring Editor
Benjamin S. Glick
University of Chicago

Received: Jul 7, 2014
Revised: Oct 17, 2014
Accepted: Oct 28, 2014

INTRODUCTION

In eukaryotic cells, the plasma membrane (PM) is a complex structure containing a plethora of lipid species (Harkewicz and Dennis, 2011). The lipids appear to be organized spatially in two major ways: phase separations in the plane of the membrane, creating microdomains (Lingwood and Simons, 2010), and, anisotropy transversely across the membrane, such that each leaflet of the bilayer has a distinct lipid composition (Fadeel and Xue, 2009). The latter property (referred to as bilayer asymmetry) was first reported for the erythrocyte PM (Gordesky, 1973) but is a property of the PM in every cell type (Devaux, 1991; van Meer, 2011). The outer leaflet of the PM contains predominantly phosphatidylcholine and sphingolipids, whereas the inner leaflet is enriched in phosphatidylethanolamine (PtdEth), phosphatidylserine (PtdSer), and phosphatidylinositol (PtdIns) and its phosphorylated derivatives (especially phosphatidylinositol 4-phosphate [PtdIns4P] and phosphatidylinositol 4,5-*bis*phosphate [PtdIns(4,5)P_2] (Devaux, 1991; Vance and Steenbergen, 2005; Fadeel and Xue, 2009). Moreover, this lipid constitution is important for many PM functions, including nutrient transport (Divito and Amara, 2009), endocytosis (Platta and Stenmark, 2011), cell signaling (Groves and Kuriyan, 2010), and cytokinesis (Emoto *et al.*, 2001; Luo *et al.*, 2009). Phosphoinositides, in particular, have been implicated in polarity establishment (Shewan *et al.*, 2011), cytoskeletal dynamics (Kapus and Janmey, 2013), membrane trafficking (Di Paolo and De Camilli, 2006),

This article was published online ahead of print in MBoC in Press (http://www.molbiolcell.org/cgi/doi/10.1091/mbc.E14-07-1193) on November 5, 2014.

Present addresses: *Max Planck Institute of Immunobiology and Epigenetics, 79108 Freiburg, Baden-Württemberg, Germany; †Bioenergy/GTL and Structural Biology Unit, Life Sciences Division, Lawrence Berkeley National Laboratory, Berkeley, CA 94710.

Address correspondence to: Jeremy Thorner (jthorner@berkeley.edu).

Abbreviations used: GFP, green fluorescent protein; KD, kinase-dead mutant; Lact, mammalian lactadherin; MAPK, mitogen-activated protein kinase; mCherry, color variant of monomeric Discoma red fluorescent protein; PH, pleckstrin homology domain; PM, plasma membrane; PtdEth, phosphatidylethanolamine; PtdIns, phosphatidylinositol; PtdIns4P, phosphatidylinositol-4-phosphate; PtdIns4,5P_2, phosphatidylinositol-4,5-*bis*phosphate; PtdSer, phosphatidylserine.

and signal transduction (Toker, 2002). The head groups of inner-leaflet glycerophospholipids recruit proteins that contain lipid-binding domains of the appropriate specificity (DiNitto *et al.*, 2003; Hurley, 2006; Moravcevic *et al.*, 2012; Stahelin *et al.*, 2014), as well as other classes of proteins containing polybasic elements (Heo *et al.*, 2006; Yeung *et al.*, 2008), membrane-insertion motifs (Antonny, 2011), or curvature-inducing scaffolds (Kozlov *et al.*, 2014).

Because of the influence that PM lipids exert on other cellular processes, how the localization and dynamics of inner-leaflet lipids are controlled is a biological question of substantial interest. In budding yeast (*Saccharomyces cerevisiae*), genetic analysis has implicated PM lipid asymmetry in several aspects of vesicle-mediated protein trafficking (Gall *et al.*, 2002; Hua *et al.*, 2002; Pomorski *et al.*, 2003; Hachiro *et al.*, 2013). Moreover, PtdIns(4,5)P_2 is enriched at highly localized sites, such as at the bud neck (Bertin *et al.*, 2010) and endocytic patches (Sun and Drubin, 2012). Similarly, a concentration of PtdSer appears to be important for proper localization of the small GTPase Cdc42 and its role in the development of cell polarity (Fairn *et al.*, 2011). Conversely, locally amassed PtdEth seems to be required for activation of the GTPase-activating proteins (GAPs) that down-regulate Cdc42-GTP (Saito *et al.*, 2007) and/or for the guanine nucleotide dissociation inhibitor (GDI)–mediated dissociation of Cdc42 from the PM (Das *et al.*, 2012).

Bilayer asymmetry, in general, and the amount of any given inner-leaflet lipid, in particular, are maintained by active inward translocation ("flipping") concomitant with similar translocation outward of exoleaflet lipids ("flopping"; Daleke, 2003; van Meer, 2011). These movements are necessary in the face of continual exocytic vesicle insertion and endocytic vesicle removal, which act to scramble leaflet lipid content. In eukaryotes, inward translocation of PtdEth and PtdSer is catalyzed by members of a subfamily (class 4) of the P-type ATPases dubbed flippases (Daleke, 2007; Tanaka *et al.*, 2011; Sebastian *et al.*, 2012; Lopez-Marques *et al.*, 2013). The *S. cerevisiae* genome encodes five flippases: Dnf1, Dnf2, Dnf3, Drs2, and Neo1 (Catty *et al.*, 1997). Paralogues Dnf1 (1571; value in parentheses indicates number of residues) and Dnf2 (1612) localize primarily in the PM, whereas Dnf3 (1656), Drs2 (1355), and Neo1 (1151) are confined mainly to intracellular membranes (Daleke, 2007; Muthusamy *et al.*, 2009). Exit of Dnf1 and Dnf2 from the ER and their insertion and function in the PM require their association with a smaller escort protein, Lem3/Ros3 (414; Kato *et al.*, 2002; Noji *et al.*, 2006); related proteins Crf1 (393; Saito *et al.*, 2004) and Cdc50 (391; Misu *et al.*, 2003; Takahashi *et al.*, 2011) serve the same function for Dnf3 and Drs2, respectively. Such a factor has not yet been identified for Neo1 (Barbosa *et al.*, 2010). Mutations in certain of the 14 human homologues of the yeast flippases (López-Marqués *et al.*, 2011) are causes of several inherited diseases (Folmer *et al.*, 2009; van der Mark *et al.*, 2013).

The role of flippases in polarized growth is particularly intriguing because the PM undergoes rapid and highly directional expansion. One known control on PM flippase function is exerted by stimulatory phosphorylation by the Ser/Thr protein kinase Fpk1. The *FPK1* gene was first identified by loss-of-function mutations synthetically lethal with a *cdc50Δ* mutation (which inactivates flippase Drs2), suggesting that Fpk1 action is needed for optimal activity of the remaining flippases. Indeed, although yeast cells lacking Fpk1 (and its paralogue, Fpk2/Kin82) are viable and did not have any change in flippase abundance or localization, they had a decreased ability to internalize fluorescently labeled PtdEth and PtdSer (Nakano *et al.*, 2008). In vitro purified Fpk1 directly phosphorylates four of the five flippases (not Neo1), with a marked preference for Dnf1 and Dnf2 (Nakano *et al.*, 2008). Fpk1 is, in turn, phosphorylated and inactivated by Ypk1 (Roelants *et al.*, 2010), a protein kinase whose function is up-regulated in response to membrane stress (Roelants *et al.*, 2011).

One biological stimulus in yeast that elicits highly polarized growth in haploid cells is exposure to mating pheromone (Segall, 1993). It was reported that PtdEth becomes detectable in the outer leaflet (Iwamoto *et al.*, 2004) and PtdSer become concentrated in the inner leaflet (Fairn *et al.*, 2011) at the leading edge of the projection (shmoo tip) that forms in pheromone-treated cells. Similarly, we demonstrated that PtdIns(4,5)P_2 becomes enriched at the same location and is required for efficient recruitment of the mitogen-activated protein kinase (MAPK) scaffold protein Ste5 and maximal MAPK signaling (Garrenton *et al.*, 2010). Hence we sought to determine whether plasma membrane lipid asymmetry and the flippases necessary to maintain it have any role in these processes. We examined the localization of the flippases and the flippase-regulating protein kinase Fpk1 upon pheromone exposure, used genetic analysis to determine that these proteins are indeed necessary for optimal pheromone response, and interrogated both wild-type and mutant cells using genetic, biochemical, and cell biological methods to determine how flippase action contributes to signal propagation.

RESULTS

Flippase localization during pheromone response

As an initial means to determine whether any flippase might contribute to PM lipid dynamics necessary for cell morphogenesis and/or signaling during pheromone response, we examined the subcellular location of these enzymes. Toward this end, we successfully fused a fluorescent marker, either green fluorescent protein (GFP; Tsien, 1998) or mCherry (Shaner *et al.*, 2004), in-frame to the C-terminal end of the chromosomal open reading frame for each of the four members of the yeast flippase family believed to reside in, or be trafficked into and out of, the PM (Daleke, 2007; Tanaka *et al.*, 2011; Sebastian *et al.*, 2012). Using appropriate complementation tests, we found that these constructs, each of which is expressed at its endogenous level from its native promoter, retained full biological function (Rockwell *et al.*, 2009; Rockwell and Thorner, unpublished results). The fifth flippase, Neo1, resides exclusively in internal membranes (Wicky *et al.*, 2004), and we found that its distribution (Supplemental Figure S1A) and level (Supplemental Figure S1B) were unaffected by pheromone treatment.

In naive cells, Dnf1-GFP and Dnf2-GFP resided in small puncta congruent with the PM disbursed reasonably uniformly around the cell periphery, especially in the PM of the bud (and, occasionally, at the bud neck), whereas the bulk of the Dnf3-GFP and Drs2-mCherry appeared to reside in cortical vesicles, in agreement with prior work indicating that Dnf3 mainly localizes to post-Golgi secretory vesicles and Drs2 in the *trans*-Golgi cisternae (Hua *et al.*, 2002; Natarajan *et al.*, 2004; Hanamatsu *et al.*, 2014; Figure 1A, left). Strikingly, within 1 h after exposure to pheromone, Dnf1-GFP, Dnf2-GFP and Dnf3-GFP were highly concentrated in the PM at the shmoo tip, whereas Drs2-mCherry remained in the Golgi compartment (Figure 1A, middle). By 90 min after exposure to pheromone, although Dnf3-GFP still showed a bias at the shmoo tip, it seemed to reside mainly in endocytic vesicles, whereas Dnf1-GFP and Dnf2-GFP persisted in the PM at the shmoo tip and Drs2-mCherry remained in the Golgi body (Figure 1A, right). These conclusions derived from standard epifluorescence microscopy were confirmed using confocal fluorescence microscopy (Supplemental Figure S2). Furthermore, immunoblot analysis of these proteins (or corresponding integrated constructs C-terminally tagged with a c-myc epitope) indicated that there was no pronounced change in the level of these proteins during the time course of pheromone treatment (Supplemental Figure S3). Thus

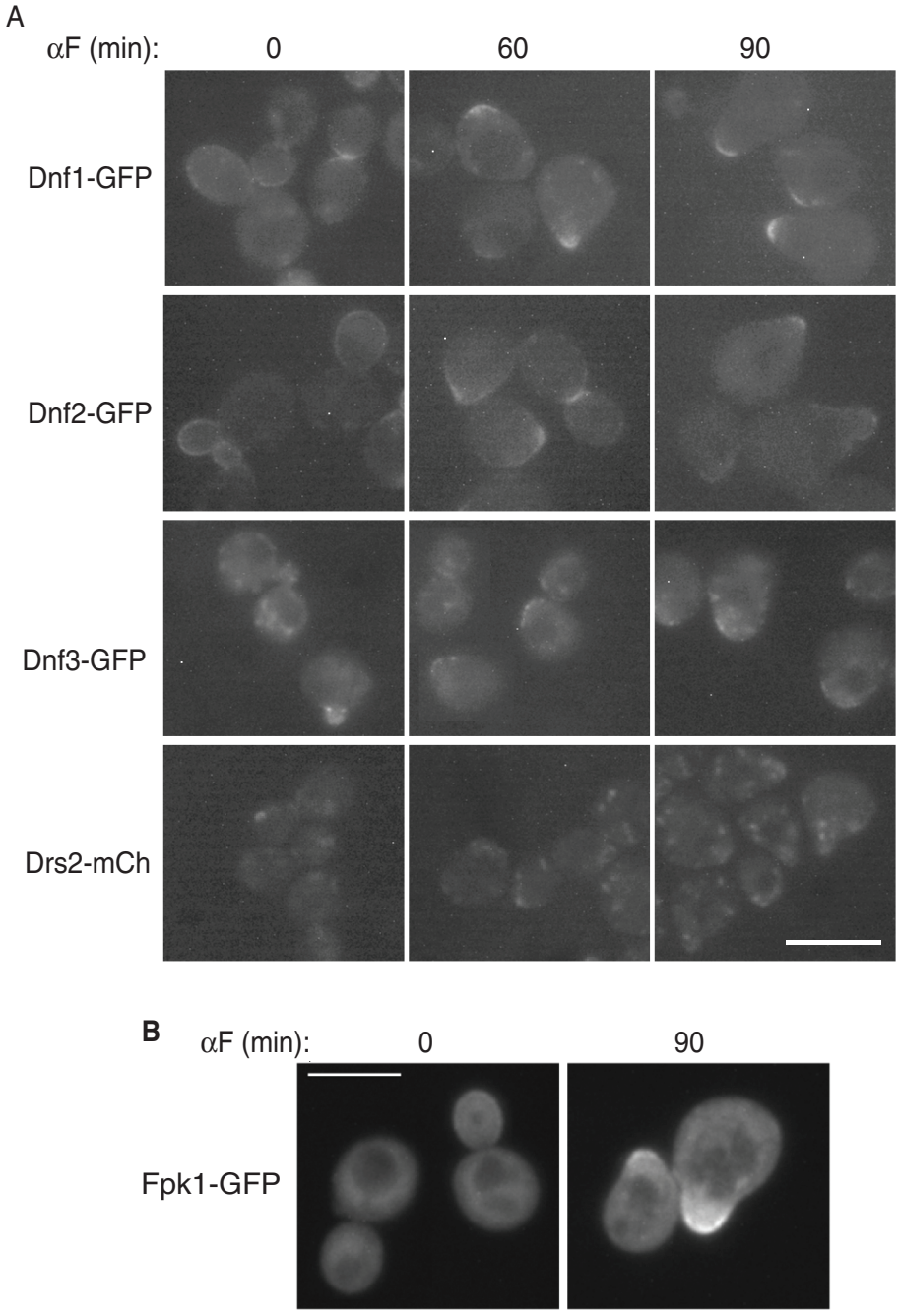

FIGURE 1: Flippase and flippase kinase localization in pheromone-treated cells. (A) *MAT***a** cells expressing the indicated flippase from its native promoter at its normal chromosomal locus as the sole source of each protein, Dnf1-GFP (NRY921), Dnf2-GFP (NRY923), Dnf3-GFP (YEB1), and Drs2-mCherry (YEB2), were grown to mid–exponential phase, exposed to α-factor (10 μM final concentration) for the indicated time, and viewed by fluorescence microscopy. (B) Cells (BY4741) expressing Fpk1-GFP from the *TPI1* promoter on a *CEN* plasmid (pFR150) were grown to mid–exponential phase in SCGlc-Leu-Trp and treated as in A. Scale bars, 5 μm.

these findings suggest that the marked relocalization exhibited by Dnf1, Dnf2, and Dnf3 places them in a position that could allow them to participate directly in membrane remodeling at the shmoo tip, the site from which signaling emanates (Garrenton *et al.*, 2010) and at which polarized growth occurs (Madden and Snyder, 1998).

The function of the flippases appears to be stimulated by the action of the protein kinase Fpk1 (and its paralogue Fpk2; Nakano *et al.*, 2008; Roelants *et al.*, 2010). Hence we used the same approach to monitor localization of Fpk1 and found that it too becomes markedly concentrated at the shmoo tip in pheromone-treated cells (Figure 1B).

Flippases are essential to induce a pheromone response

To test whether the observed relocalizations are functionally significant and not merely the consequence of the highly directional secretion and cell growth that occurs during projection formation, we tested whether null alleles in one or more of these genes had any effect on the ability of the cells to respond to pheromone. This analysis was possible because, aside from Neo1, which is an essential gene (Prezant *et al.*, 1996), cells carrying complete deletions of any of the other four flippases, and even of any three together, are viable, although a *dnf1Δ dnf2Δ dnf3Δ drs2Δ* quadruple mutant is inviable (Hua *et al.*, 2002), indicating a significant degree of overlap in the physiological roles of these proteins. As a first means to assess pheromone responsiveness, we examined the frequency of shmoo formation in cultures of various combinations of *dnf1Δ*, *dnf2Δ*, *dnf3Δ*, and *drs2Δ* null alleles. As anticipated, no single deletion mutant displayed any significant defect in its efficiency of shmoo formation upon α-factor treatment (Figure 2A), in keeping with the apparent redundancies in localization and function of these flippases (Daleke, 2007; Sebastian *et al.*, 2012). Indeed, even double-mutant combinations exhibited little or no reduction in shmoo formation or only a very modest (twofold) decrease, in the case of *dnf3Δ drs2Δ* cells (Figure 2A). In contrast, and in agreement with a largely shared function, we found that two triple mutants, *dnf1Δ dnf3Δ drs2Δ* and especially *dnf1Δ dnf2Δ dnf3Δ*, had a marked reduction in their ability to form a shmoo (Figure 2A).

The defect in shmoo formation exhibited by the two triple mutants we examined could arise from a defect in cell morphogenesis or from an inability to mount a pheromone response of any sort. To distinguish between these possibilities, we also monitored pheromone response by an independent assay, namely the ability to induce expression of a pheromone-responsive reporter gene, *FUS1* (Trueheart *et al.*, 1987). For this purpose, a single copy of a *FUS1* promoter-driven *lacZ* construct was integrated at the *FUS1* locus in the two triple mutants and in otherwise isogenic wild-type cells as a control. As observed for shmoo formation, even 60 min after pheromone treatment, the *dnf1Δ dnf3Δ drs2Δ* cells and especially the *dnf1Δ dnf2Δ dnf3Δ* showed a dramatic reduction in reporter gene expression (Figure 2B). Thus the defect in shmoo formation was attributable to a lack of signaling, regardless of whether the flippases may also have some role in the PM remodeling that may accompany highly polarized growth.

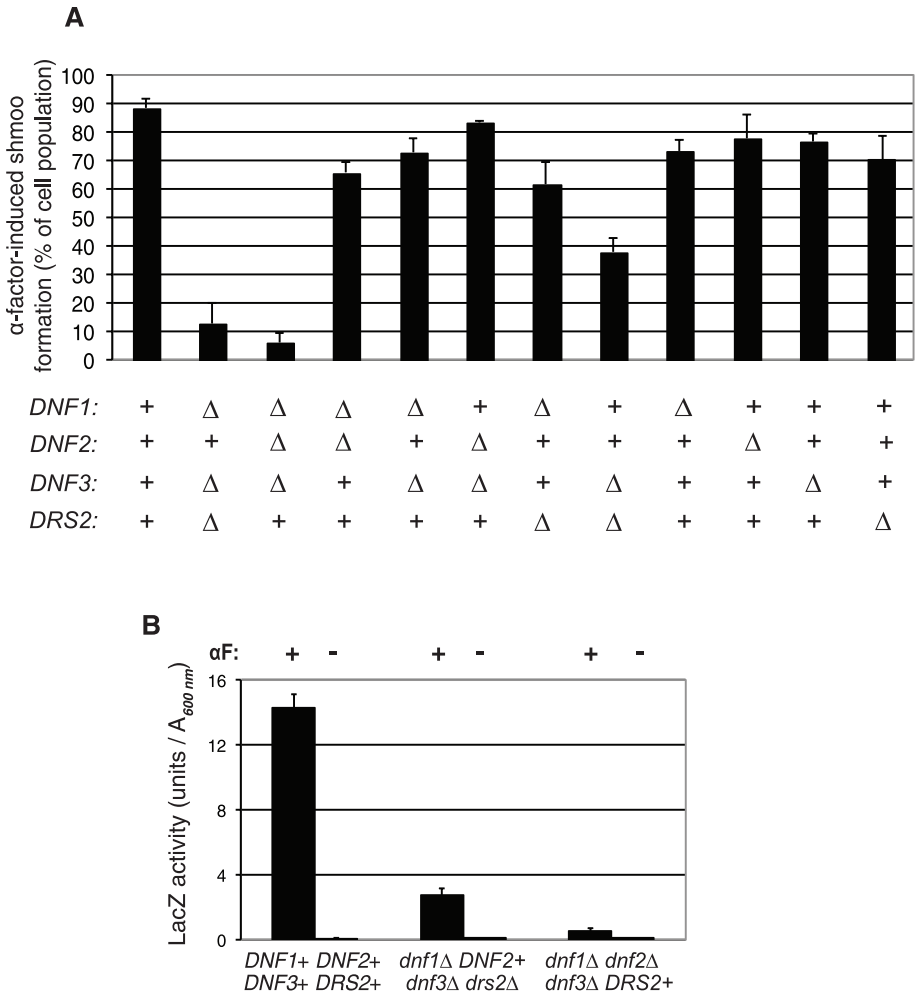

FIGURE 2: Deletion of multiple flippases with overlapping function impairs pheromone response. (A) Exponentially growing cultures of cells of the indicated genotype (see Table 1) were exposed to 10 μM α-factor for 1.5 h and examined by microscopy. Values are the mean ± SD of three independent experiments. (B) WT (YLG32), *dnf1Δ dnf3Δ drs2Δ* (YELO4), and *dnf1Δ dnf2Δ dnf3*Δ (YELO3) cells expressing a copy of a $FUS1_{prom}$-*lacZ::URA3* reporter (pSB286) integrated at the *FUS1* locus were grown to mid–exponential phase, collected, resuspended in either YPD or YPD plus 10 μM α-factor, and, after 60 min, assayed for galactosidase activity. Values are the mean ± SD from three independent experiments.

If flippase activity is critical for induction of pheromone response and the flippases require phosphorylation and activation by Fpk1 and Fpk2 for their optimal activity (Nakano *et al.*, 2008), then even otherwise wild-type cells (i.e., with a full complement of flippases) may have a defect in pheromone response if they lack these flippase-activating protein kinases. Consistent with this view, loss of neither Fpk1 alone nor Fpk2 alone had any significant effect on the efficiency of shmoo formation by otherwise wild-type cells, whereas an *fpk1Δ fpk2Δ* double mutant exhibited a pronounced decrease (Figure 3A). In this same regard, we described before that Fpk1 and Fpk2 are subject to inhibitory phosphorylation by the protein kinase Ypk1 (Roelants *et al.*, 2010). Hence we used high-level overexpression of Ypk1 as an independent means to impede Fpk1 and Fpk2 activity in otherwise wild-type cells and found that this tactic also caused a statistically significant drop in the frequency of shmoo formation, whereas neither empty vector nor a catalytically crippled mutant Ypk1(K376A; Roelants *et al.*, 2004) had any obvious effect (Figure 3B). Collectively these findings indicated that flippase action contributes in some way to the competence of the cells to respond to pheromone. Hence we sought to determine what aspect of signal initiation or propagation is impaired in flippase-deficient cells.

Ste5 level is dramatically reduced in *dnf1Δ dnf2Δ dnf3Δ* cells

All the initial steps of the mating pheromone response pathway take place in, or on the cytosolic surface of, the PM (Merlini *et al.*, 2013). Activation of the pathway in *MAT***a** cells is triggered by binding of α-factor pheromone to its cognate G protein–coupled receptor, Ste2 (Blumer *et al.*, 1988). It was reported recently in *Drosophila* that there was a marked reduction in the amount of an olfactory receptor (Or67d) inserted into the PM in the cilia on specific olfactory neurons that sense a male-specific pheromone in a mutant lacking the apparent fly orthologue (dATP8B) of mammalian flippase ATP8B1 (Ha *et al.*, 2014), whose apparent homologues in *S. cerevisiae* are Dnf1 and Dnf2 (Folmer *et al.*, 2009; van der Mark *et al.*, 2013). To test whether the amount of Ste2 delivered to the PM was affected in either of the yeast flippase triple mutants, we examined Ste2 localization in cells expressing a C-terminally mCherry-tagged version of the Ste2(7K-to-R) allele, which we demonstrated previously is functional but has markedly retarded ubiquitin-dependent endocytosis (Ballon *et al.*, 2006), making it easier to score the steady-state level of receptor in the PM. We found that delivery of Ste2(7K-to-R)-mCherry to the PM was not defective in either *dnf1Δ dnf2Δ dnf3Δ* (Figure 4A) or *dnf1Δ dnf3Δ drs2Δ* cells (unpublished data); in fact, the level of Ste2(7K-to-R)-mCherry appeared to be somewhat higher in the *dnf1Δ dnf2Δ dnf3Δ* mutant than in the corresponding control, consistent with the retardation of endocytosis described previously for cells deficient in both Dnf1 and Dnf2, especially at lower temperatures (Pomorski *et al.*, 2003). Hence lack of PM-localized Ste2 cannot account for the inability of the multiply flippase-deficient cells to respond to pheromone.

Focusing here, first, on the underlying cause of the inability of the *dnf1Δ dnf2Δ dnf3Δ* cells to respond to pheromone, we took advantage of the fact that ectopic overexpression of the pheromone receptor–associated Gβγ complex (Ste4–Ste18) is known to induce all pathway outputs even in the absence of pheromone (Cole *et al.*, 1990; Whiteway *et al.*, 1990). Hence, if the signaling defect lies at or downstream of Gβγ action, then the *dnf1Δ dnf2Δ dnf3Δ* mutant should be unresponsive to Ste4–Ste18 overexpression. However, we found no statistically significant difference between the *dnf1Δ dnf2Δ dnf3Δ* cells and otherwise isogenic controls cells in shmoo formation (Figure 4B) or any other readout of pheromone response (unpublished data) when Gβγ was overexpressed. Therefore we concentrated our attention on the factors that act at the nexus between receptor activation and the function of Gβγ.

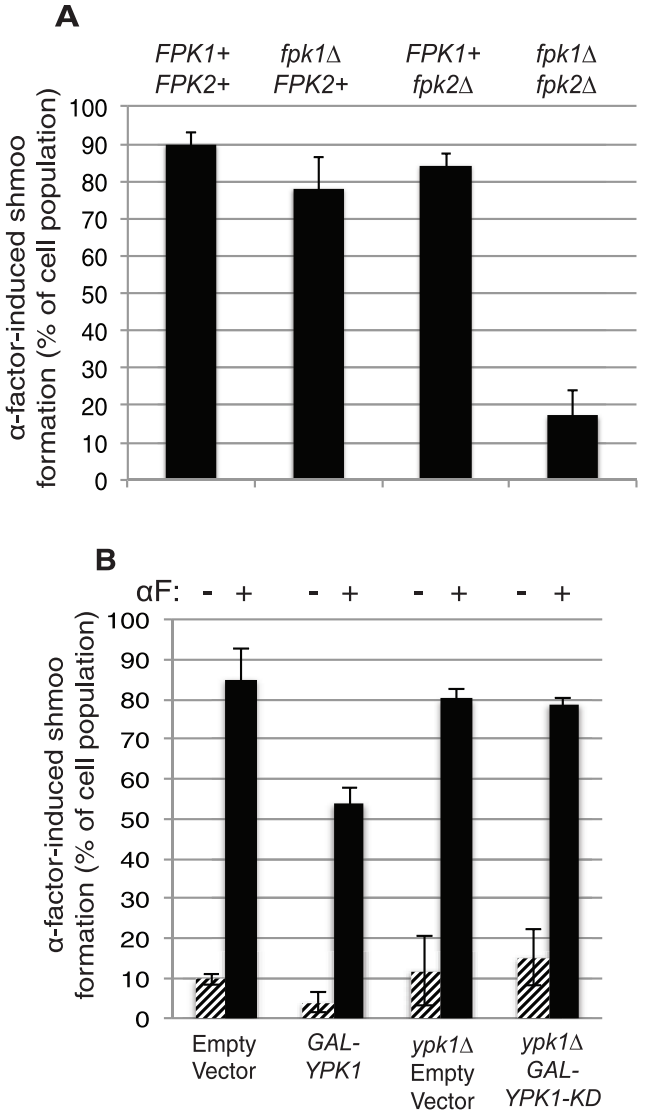

FIGURE 3: Fpk1 and Fpk2 function are required for optimal pheromone response. (A) Cultures of WT (BY4741), *fpk1*Δ (YFR191), *fpk2*Δ (YFR222), and *fpk1*Δ *fpk2*Δ (YFR205) cells were grown to mid–exponential phase in YPD medium, treated with 10 μM α-factor for 1.5 h, and examined by microscopy. (B) WT cells (BY4741) carrying empty vector (YEp352GAL) or the same vector overexpressing Ypk1 (pAM76), or *ypk1Δ* cells (JTY6142) carrying YEp352GAL or the same vector overexpressing a KD mutant, Ypk1(K376), were grown to mid–exponential phase in SC-Ura+Raf/Suc medium, collected, and resuspended in SC-Ura+Gal medium, grown for an additional 3 h, incubated in the absence and presence of 10 μM α-factor for 1.5 h, and examined by microscopy. Values are the mean ± SD from three independent experiments.

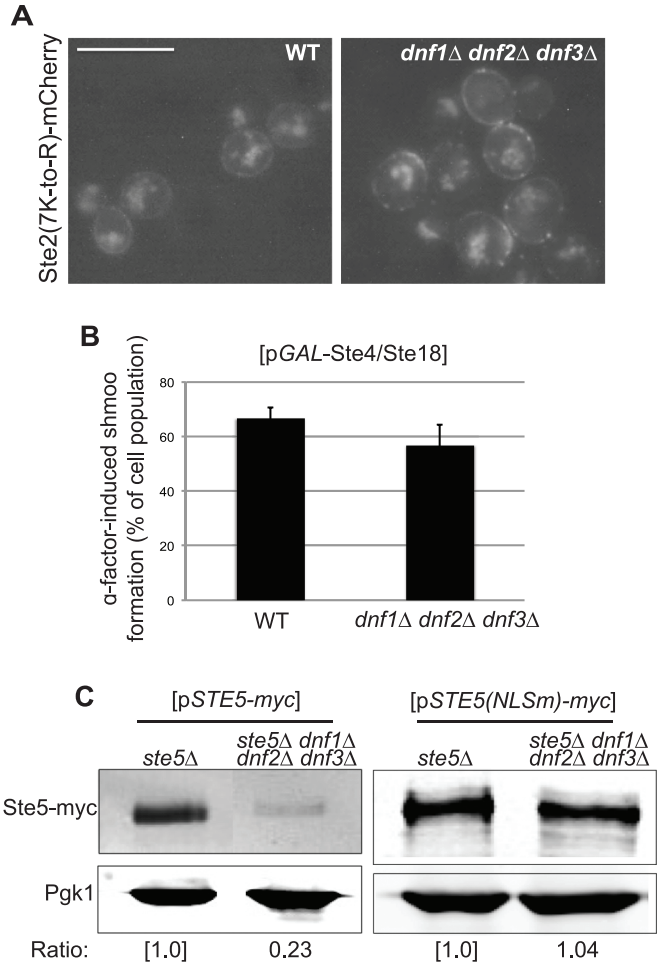

FIGURE 4: Steady-level of Ste5 is markedly decreased in *dnf1Δ dnf2Δ dnf3*Δ cells. (A) WT (YELO17) and *dnf1Δ dnf2Δ dnf3*Δ (YELO18) cells expressing Ste2(7K-to-R)-mCherry from the *STE2* promoter at the *STE2* locus were grown to mid–exponential phase in YPD and examined by fluorescence microscopy. Scale bar, 10 μm. (B) WT (BY4741) and *dnf1Δ dnf2Δ dnf3*Δ cells (PFY3272C) carrying plasmid pRS316-*GAL-STE4/STE18* were grown to mid–exponential phase in SC-Ura+Raf/Suc medium, collected, resuspended in SC-Ura+Gal, and examined after 8 h by microscopy. Values are the mean ± SD from three independent trials. (C) Cultures of *ste5Δ* (YELO23) and *ste5Δ dnf1Δ dnf2Δ dnf3Δ* (YELO24) expressing either Ste5-myc from plasmid p$STE5_{prom}$-*STE5-myc*$_{13}$ or Ste5(NLSm)-myc from plasmid p$STE5_{prom}$-*ste5(NLSm)-myc*$_{13}$ were grown to mid–exponential phase in SCGlc-Ura medium, collected, and lysed, and equal amounts of protein of the resulting whole-cell extracts were resolved by SDS–PAGE and analyzed by blotting with anti-myc monoclonal antibody and anti-Pgk1 as a loading control. Left, the lanes shown were separated on the original gel and have been spliced together here for clarity.

Paramount among these factors is the MAPK cascade scaffold protein Ste5, whose signaling function requires its efficient recruitment to and stable association with the PM via insertion of an N-terminal amphipathic helix (Winters *et al.*, 2005), interaction of its RING domain with Gβγ (Inouye *et al.*, 1997), and binding of its PH domain to PtdIns(4,5)P_2 (Garrenton *et al.*, 2006). Moreover, ample evidence implicates Ste5 as the rate-limiting component for initiation and maintenance of pheromone-evoked MAPK signaling (Takahashi and Pryciak, 2008; Garrenton *et al.*, 2009; Thomson *et al.*, 2011). Strikingly, immunoblot analysis (Figure 4C, left) revealed that the steady-state level of Ste5 was markedly lower in the *dnf1Δ dnf2Δ dnf3Δ* mutant than in otherwise isogenic control cells and presumably below the threshold adequate for most cells in the population to mount an effective pheromone response. The decrease in Ste5 could be due either to a lower level of expression or to a higher rate of degradation (or both). Analysis of the level of Ste5 mRNA by quantitative reverse transcriptase-PCR showed that the amount of Ste5 transcript in *dnf1Δ dnf2Δ dnf3*Δ cells was indistinguishable from that in WT cells (unpublished data), indicating that the reduction in Ste5 protein was likely due to an increase in its rate of turnover.

Ste5, which undergoes robust nucleocytoplasmic shuttling (Pryciak and Huntress, 1998; Mahanty *et al.*, 1999; Künzler *et al.*, 2001), is targeted for degradation exclusively in the nucleus by the nuclearly localized ubiquitin:protein ligase (E3) SCF^{Cdc4} (Garrenton *et al.*, 2009). Once sufficient Cln2 has built up to initiate the cell cycle, the cell is no longer susceptible to pheromone because Cln2-bound Cdk1/Cdc28 phosphorylates any PM-associated Ste5, ejecting it from the PM (Strickfaden *et al.*, 2007), thus allowing it to translocate into the nucleus and be degraded (Garrenton *et al.*, 2009). We reasoned that if the lower steady-state level of Ste5 displayed by *dnf1Δ dnf2Δ dnf3Δ* cells was due to an enhanced rate of its degradation in the nucleus, then point mutations that eliminate the major nuclear localization signal (NLS) in Ste5 (Strickfaden *et al.*, 2007) might suppress the effect on Ste5 level observed in the multiple flippase–deficient cells. Indeed, when its major NLS was mutationally crippled, the steady-state level of Ste5 in *dnf1Δ dnf2Δ dnf3Δ* cells was restored to that seen in control cells (Figure 4C, right). Therefore our attention turned to finding some mechanistic explanation for how loss of Dnf1, Dnf2, and Dnf3 might influence the processes that dictate Ste5 stability.

Factors contributing to Ste5 instability in *dnf1Δ dnf2Δ dnf3Δ* cells

Because the action of G1 cyclin-bound Cdk1/Cdc28 displaces Ste5 from the PM, permitting its nuclear entry and degradation, we first asked whether there was any effect of the loss of Dnf1, Dnf2, and Dnf3 on the level of Cln2. Unexpectedly, we observed even in asynchronous cultures a modest but reproducible increase in the steady-state level of this G1 cyclin in *dnf1Δ dnf2Δ dnf3Δ* cells compared with the WT control (Figure 5A). As an independent means to determine whether this moderate increase was enough to contribute to the lower level of Ste5 seen in *dnf1Δ dnf2Δ dnf3Δ* cells, we reduced the total G1 cyclin-producing capacity of the cell by deleting both the *CLN1* and *CLN3* genes. This tactic more than doubled the relative level of Ste5 in *dnf1Δ dnf2Δ dnf3Δ* cells (Figure 5B) and, consistent with the elevation in Ste5 content, partially restored (a threefold increase) the ability of the cell population to respond to pheromone (Figure 5C).

We noted that a majority of the *dnf1Δ dnf2Δ dnf3Δ* cells exhibited buds whose axial ratio was somewhat more elongated than in the corresponding wild-type cells (Supplemental Figure S4; see also, e.g., Figure 6A). This morphological response can arise when the amount or activity of the cyclin B (Clb)–bound form of Cdk1/Cdc28 is compromised (Howell and Lew, 2012). Moreover, because Clb2-Cdk1 is known to phosphorylate and inhibit the SBF transcription factor required for expression of the G1 cyclin genes (Amon *et al.*, 1993), a lower level of Clb-bound Cdk1 might explain the higher level of Cln2 we observed in *dnf1Δ dnf2Δ dnf3Δ* cells. Consistent with this view, we found a modest but reproducible reduction in the cellular content of Clb2 in the *dnf1Δ dnf2Δ dnf3Δ* cells as compared with the cognate control cells (Supplemental Figure S5).

One of the components required for bud emergence and timely progression through the apical-to-isotropic switch in bud expansion is the small Rho-family GTPase Cdc42 (Bi and Park, 2012). It has been shown that Dnf1- and Dnf2-catalyzed PtdEth flipping to the inner leaflet is required for activation of the GAPs Rga1 and Rga2 that down-regulate Cdc42-GTP (Saito *et al.*, 2007; and/or for the Rdi1-mediated dissociation of Cdc42 from the PM; Das *et al.*, 2012). In cells lacking Lem3 (the required escort protein and cofactor for Dnf1 and Dnf2), polarized Cdc42 persists, leading to continued apical bud growth at low temperatures, resulting in an elongated bud (Saito *et al.*, 2007). Presumably the flippase defect of *dnf1Δ dnf2Δ dnf3Δ* cells is even greater than of *lem3Δ* cells, given that these cells manifest somewhat enlarged and elongated buds even at 30°C (Figure 6A, left). It has also been reported that another flippase substrate, PtdSer, accumulates at bud necks, in the bud cortex, and at the tips of mating projections and that a PtdSer synthase (*cho1Δ/pss1Δ*) mutant has impaired polarization of Cdc42, causing a delay in bud emergence and defective mating (Fairn *et al.*, 2011).

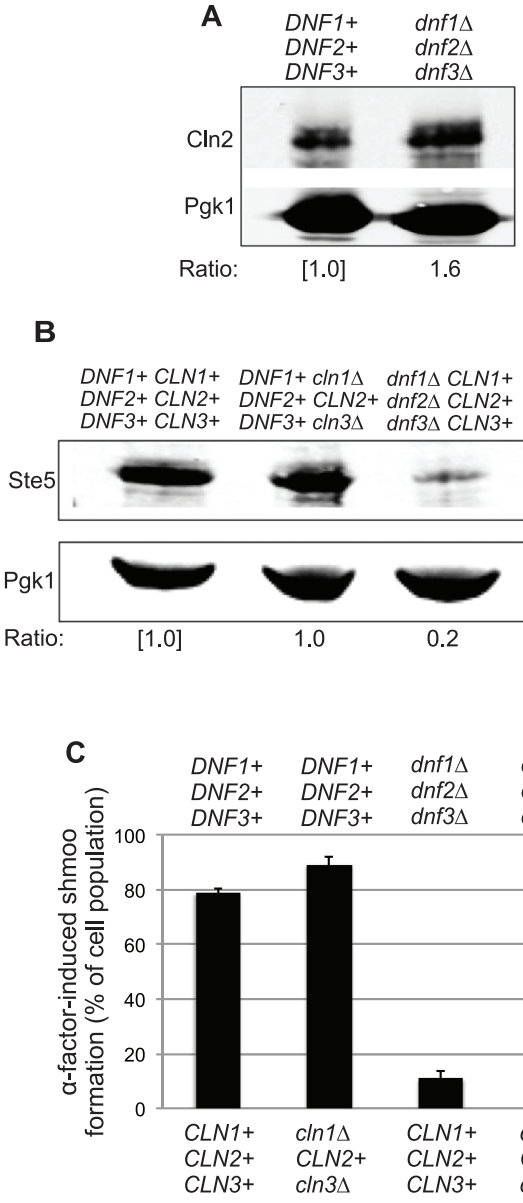

FIGURE 5: Reduction in G1 cyclin activity partially rescues Ste5 protein level and pheromone responsiveness in *dnf1Δ dnf2Δ dnf3Δ* cells. (A) WT (BY4741) and derived *dnf1Δ dnf2Δ dnf3Δ* cells (PFY3272C) were grown to mid–exponential phase in YPD, collected, and lysed, and equal amounts of protein from the whole-cell extracts were resolved by SDS–PAGE and analyzed by immunoblotting with appropriate antibodies. Representative blot from three independent trials. (B) As in A, for WT, *cln1Δ cln3Δ* (YELO38), *dnf1Δ dnf2Δ dnf3Δ* (PFY3272C), and *cln1Δ cln3Δ dnf1Δ dnf2Δ dnf3Δ* (YELO39) cells. (C) WT (BY4741) and *cln1Δ cln3Δ* (YELO38), *dnf1Δ dnf2Δ dnf3Δ* (PFY3272C), and *cln1Δ cln3Δ dnf1Δ dnf2Δ dnf3Δ* (YELO39) cells were incubated with 10 μM α-factor for 1.5 h and examined by microscopy. Values are mean ± SD from three independent experiments.

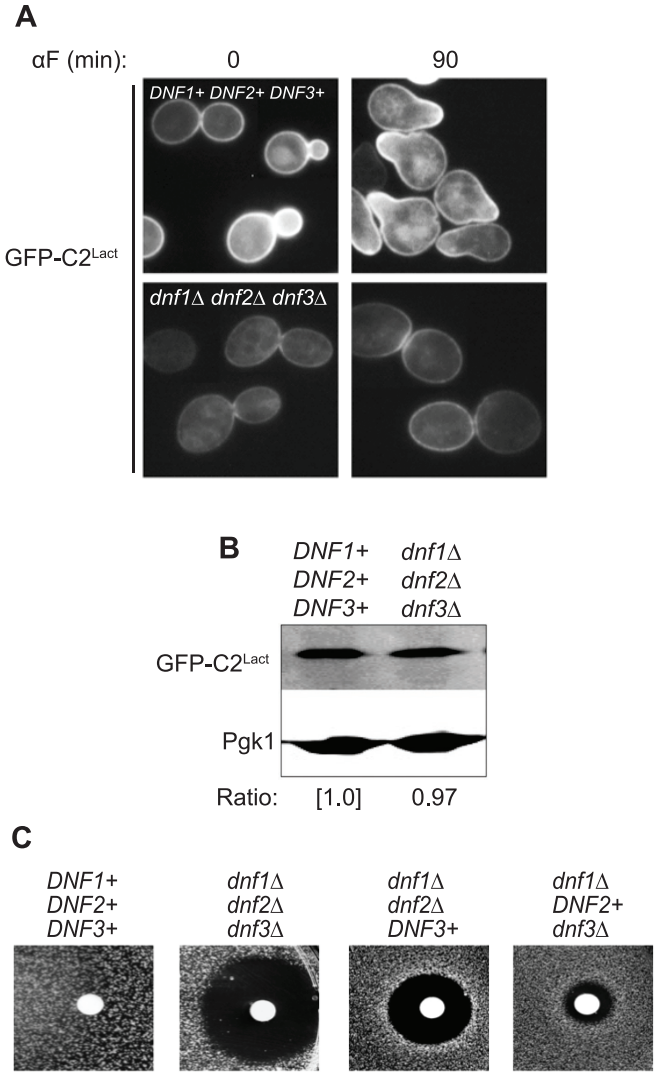

FIGURE 6: Flippase function increases inner-leaflet PtdSer and lowers outer-leaflet PtdEth. (A) WT (BY471) and isogenic *dnf1Δ dnf2Δ dnf3Δ* (PFY3272C) cells carrying a *URA3*-marked *CEN* plasmid expressing GFP-C2^{Lact} from the *TDH3* (GAPDH/GPD) promoter were grown to mid–exponential phase in SCGlc-Ura medium, treated with 10 μM α-factor, and examined by fluorescence microscopy at the indicated time. (B) Cells shown in A were lysed, and equivalent amounts of protein from the whole-cell extracts were resolved by SDS–PAGE and analyzed with anti-GFP antibodies to detect the GFP-C2^{Lact} fusion protein and anti-Pgk1 antibodies as the loading control. (C) Equivalent numbers of WT (BY4741), isogenic *dnf1Δ dnf2Δ dnf3Δ* (PFY3272C), *dnf1Δ dnf2Δ* (YELO9), *dnf1Δ dnf3Δ* (YELO10), and *dnf2Δ dnf3Δ* (YEL013) cells were each plated as a lawn in top agar on YPD plates, and sterile filter paper disks onto which 10 μl of a stock solution (8 mM) of duramycin had been spotted were immediately placed onto the lawn. After incubation for 2 d at 30°C, the plates were photographed. Response of *dnf2Δ dnf3Δ* cells (not shown) closely resembled that of *dnf1Δ dnf3Δ* cells.

To examine inner-leaflet PtdSer, we expressed, as a fusion to GFP, the C2 domain of the mammalian protein lactadherin (also known as MFG-E8), which is specific for binding to the head group of PtdSer (Shao *et al.*, 2008; Yeung *et al.*, 2008; Ye *et al.*, 2013). As expected, when compared with otherwise isogenic control cells, there was a marked decrease (nearly 60%) in the intensity of PM labeling with this probe in *dnf1Δ dnf2Δ dnf3Δ* cells, both before and after pheromone treatment (Figure 6A; average PM pixel intensity per unit area [n = 100 cells]: WT, 3.2 ± 0.8; *dnf1Δ dnf2Δ dnf3Δ*, 1.4 ± 0.4). Immunoblotting demonstrated that the difference in PM decoration by GFP-C2^{Lact} was not due to any difference in expression of this probe (Figure 6B). Thus, in the triple mutant, inward movement of PtdSer appears to be highly defective.

There is no corresponding genetically encoded probe to assess inner-leaflet PtdEth. Hence we used an indirect measure of the efficiency of PtdEth translocation from the outer to the inner leaflet. The killing action of the antibiotic duramycin involves its specific binding to PtdEth on the exocellular surface of the PM (Zhao, 2011). Hence the more PtdEth in the outer leaflet, the more sensitive a yeast cell is to duramycin (Roelants *et al.*, 2010). Using an agar diffusion bioassay (Figure 6C), we indeed found that, at a concentration of duramycin that has no effect on wild-type cells, the *dnf1Δ dnf2Δ dnf3Δ* triple mutant displayed a large zone of cell death, and analysis of double mutants indicated that Dnf1 and Dnf2 are the flippases primarily responsible for the inward movement of PtdEth.

Presumably, in the absence of sufficient inner-leaflet PtdSer, Cdc42 is less efficiently recruited to the PM; however, whatever PM-associated Cdc42-GTP is there will have a more protracted lifetime because, in the absence of sufficient inner-leaflet PtdEth, GAP and GDI activity will be less efficient. As one means to assess which of these two effects is the more dominant, we examined the subcellular localization of the Cdc42 GEF (Cdc24) because there is ample evidence that Cdc42-GTP participates in a self-reinforcing positive feedback loop to stably recruit Cdc24 to the site of apical bud growth (Bose *et al.*, 2001; Gulli and Peter, 2001; Butty *et al.*, 2002). Indeed, we found (Supplemental Figure S6) that, compared with the control, in the *dnf1Δ dnf2Δ dnf3Δ* cultures a much larger fraction of the cells with medium or large buds had readily detectable GFP-Cdc24 at the site of apical bud growth, which suggests that GAP- and/or GDI-mediated down-regulation of Cdc42-GTP is impaired. At this time, however, how this mild morphogenetic anomaly may be connected to the slightly elevated Cln2 and slightly reduced Clb2 level observed in *dnf1Δ dnf2Δ dnf3Δ* cells is unclear, aside from the fact that perturbations of Cdc42 function might be expected to delay cell cycle progression.

Recruitment of Ste5 to the plasma membrane is impaired in *dnf1Δ dnf2Δ dnf3Δ* cells

If the primary defect in mounting an efficacious pheromone response in *dnf1Δ dnf2Δ dnf3Δ* cells is due to the low level of Ste5, then ectopic overexpression from a strong promoter should ameliorate the problem. Toward this end, we overexpressed *STE5* from the *GAL1* promoter on a multiple-copy plasmid in *dnf1Δ dnf2Δ dnf3Δ* cells and indeed found that the fraction of the population competent to form robust shmoos in response to α-factor treatment was increased by an order of magnitude, from 4% (Figure 2A) to >40% (Figure 7A, left). However, we noted that the frequency of shmoo formation was still not at the level displayed by wild-type cells in either the absence (Figure 2A) or presence of overexpressed *STE5* (Figure 7A, left). Hence we overexpressed in the same manner a mutant allele of Ste5, Ste5(P44L) (Sette *et al.*, 2000), which has been shown to enhance association of Ste5 with the PM (Winters *et al.*, 2005). Although this construct was slightly toxic to the cells, the efficiency of shmoo formation by the *dnf1Δ dnf2Δ dnf3Δ* cells was now equivalent to that exhibited by the wild-type cells (Figure 7A, middle), suggesting that, in addition to the lower steady-state level of Ste5 in *dnf1Δ dnf2Δ dnf3Δ* mutants, the lack of these flippase creates a PM milieu that is less conducive to Ste5 recruitment. However, when overexpressed, the GFP-tagged versions of both

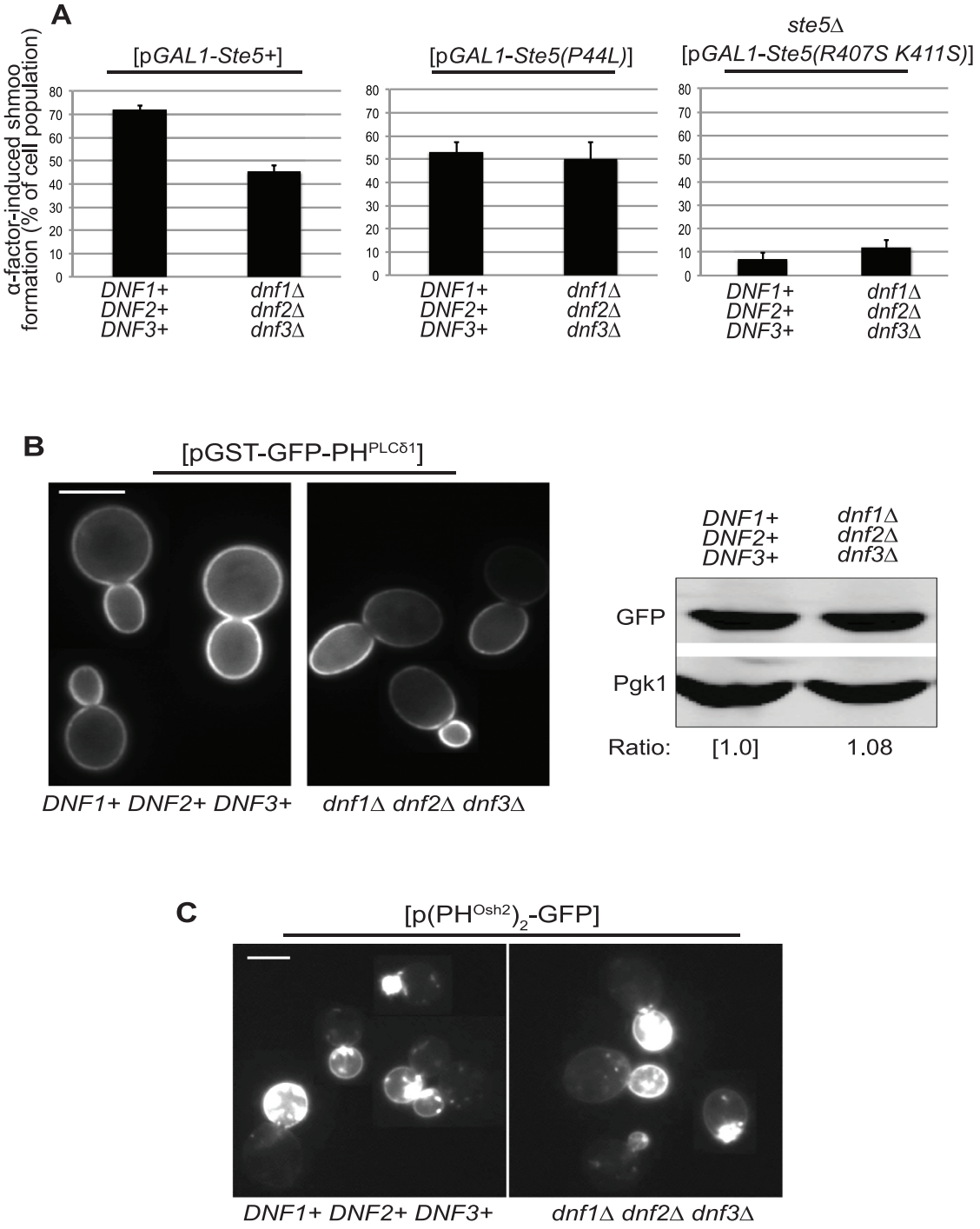

FIGURE 7: Ste5 tethering at the PM is disturbed in *dnf1Δ dnf2Δ dnf3Δ*. (A) Either WT (BY4741) or *dnf1Δ dnf2Δ dnf3Δ* cells (PFY3272C) overexpressing from the *GAL1* promoter either Ste5 (pCJ6) or Ste5(P44L) (pCS7), as indicated, from *URA3*-marked, YEp352-derived plasmids, and *ste5Δ* derivatives of the same strains overexpressing Ste5(R407S K411S) from the same vector, which were grown to mid–exponential phase in SCGlc-Ura, collected, resuspended in SCGal-Ura, propagated for 3–4 h, incubated with 10 μM α-factor for 1.5 h, and examined in the microscope. Values are the mean ± SD from three independent trials. (B) Left, a *URA3*-marked *CEN* plasmid (pPP1872) expressing the PtdIns(4,5)P_2-specific probe GST-GFP-PH$^{PLC\delta1}$ was introduced into the control and the *dnf1Δ dnf2Δ dnf3Δ* mutant, which were then treated as in A and viewed by fluorescence microscopy. Scale bar, 5 μm. Right, samples of the same cells were lysed, and equivalent amounts of protein from the whole-cell extracts were resolved by SDS–PAGE and analyzed by immunoblot with appropriate antibodies. (C) As in B, except that the *URA3*-marked *CEN* plasmid expressed the PtdIns4P-specific probe 2XPH^{Osh2}-GFP.

wild-type Ste5 and the constitutively active Ste5(P44L) allele were recruited to the shmoo tip in the pheromone-treated cells (Supplemental Figure S7).

To initiate and maintain a signal in response to pheromone, recruitment of Ste5 to the PM requires binding of its PH domain to PtdIns(4,5)P_2 (Garrenton *et al.*, 2006, 2010). Indeed, in the absence

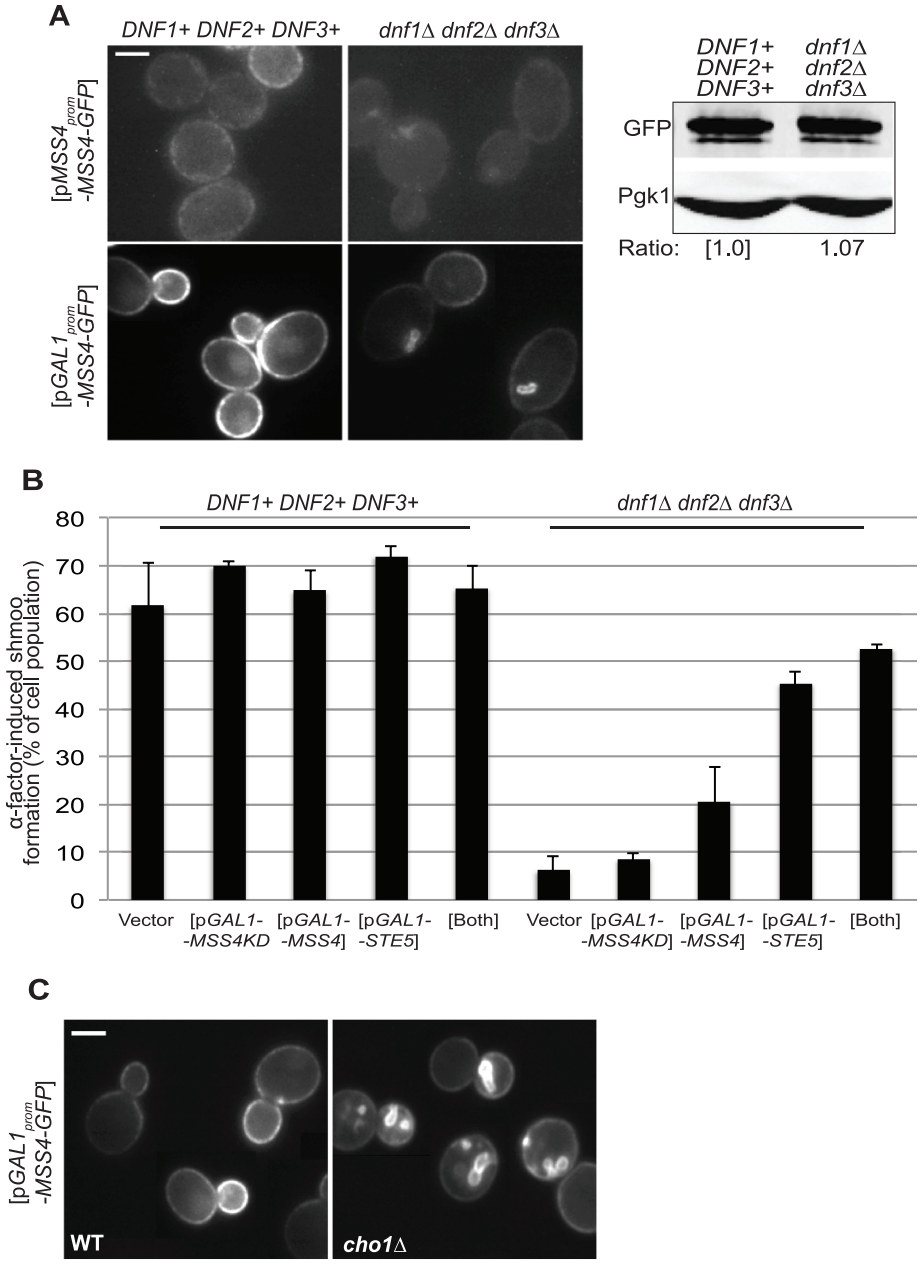

FIGURE 8: Mislocalization of Mss4 in *dnf1Δ dnf2Δ dnf3Δ* cells. (A) Left, *URA3*-marked *CEN* plasmids expressing Mss4-GFP from the *MSS4* promoter (pCS321; top) or from the *GAL1* promoter (pRB2; bottom) were introduced into WT (BY4741) and *dnf1Δ dnf2Δ dnf3Δ* (PFY3272C) cells. The resulting transformants were grown to mid–exponential phase in SCGlc-Ura (top) or shifted to SCGal-Ura for 3 h (bottom) and then examined by fluorescence microscopy. Scale bar, 5 μm. Right, samples of the same cells were lysed, and equivalent amounts of protein from the whole-cell extracts were resolved by SDS–PAGE and analyzed by immunoblot with appropriate antibodies. (B) WT and *dnf1Δ dnf2Δ dnf3Δ* cells were transformed with an empty *LEU2*-marked multicopy vector (YEp351GAL) or the same vector expressing from the *GAL1* promoter *MSS4* (pES4), a catalytically inactive (KD) allele Mss4(D636A) (pES20), a *URA3*-marked multicopy vector expressing *STE5* from the *GAL1* promoter (pCJ6), or both the *MSS4*- and *STE5*-expressing plasmids together. The resulting transformants were grown to mid–exponential phase in SCGlc-Leu, SCGlc-Ura, or SCGlc-Leu-Ura, as appropriate, collected, resuspended in SCGal-Leu, SCGal-Ura, or SCGal-Leu-Ura for 3 h, incubated with 10 μM α-factor for 1.5 h, and examined by microscopy. Values are mean ± SD from three independent experiments. (C) WT (BY4741) and otherwise isogenic *cho1Δ* (JTY6525) carrying a plasmid (pRB2) expressing *MSS4* under control of the *GAL1* promoter were grown to mid–exponential phase in SCGal-Ura and examined by fluorescence microscopy. Scale bar, 5 μm.

of endogenous Ste5, overexpression of a Ste5 mutant, Ste5(R407S K411S), unable to interact stably with the PM due to lack of a functional PH domain (Garrenton *et al.*, 2006, 2010), was unable to support robust shmoo formation in either wild-type or *dnf1Δ dnf2Δ dnf3Δ* cells (Figure 7A, right). As one means to assess PM PtdIns(4,5)P_2 content and distribution, we first examined localization of a fluorescence probe (GST-GFP-PH$^{PLC\delta1}$) that contains the PH domain derived from mammalian PLCδ1, which is highly specific for recognition of PtdIns(4,5)P_2 (Stauffer *et al.*, 1998; Szentpetery *et al.*, 2009). We observed that, compared with control cells, the *dnf1Δ dnf2Δ dnf3Δ* mutant exhibited both a reduction in overall intensity and much less decoration of the PM in mother cells than in buds (Figure 7B, left). Immunoblotting of the same cells showed that this difference was not attributable to any difference in the level of probe expression (Figure 7B, right). By contrast, using a PtdIns4P-specific probe that contains tandem copies of the PH domain of yeast Osh2 (Roy and Levine, 2004), we did not observe any difference in either intensity or pattern between control cells and *dnf1Δ dnf2Δ dnf3Δ* mutant (Figure 7C).

Mss4 is mislocalized in *dnf1Δ dnf2Δ dnf3Δ* cells

PtdIns4P is converted to PtdIns(4,5)P_2 by the sole PtdIns4P 5-kinase in yeast Mss4 (Audhya and Emr, 2003; Strahl and Thorner, 2007), and an *mss4^{ts}* mutant fails to recruit Ste5 to the PM and is unable to respond to pheromone at the nonpermissive temperature (Garrenton *et al.*, 2010). When Ste5 cannot be stably tethered at the PM, it is subject to rampant degradation in the nucleus (Garrenton *et al.*, 2009). Hence inefficient generation of PM PtdIns(4,5)P_2 could explain both the lower level of Ste5 and the signaling defect observed in *dnf1Δ dnf2Δ dnf3Δ* cells. For these reasons, we examined the subcellular localization of Mss4.

When expressed at a near-endogenous level (from its native promoter on a *CEN* plasmid) in wild-type cells, Mss4-GFP decorated the inner perimeter of the PM as a series of bright puncta, as observed before (Audhya and Emr, 2003), whereas in *dnf1Δ dnf2Δ dnf3Δ* cells, the intensity of the PM decoration was reduced by >70% (average PM pixel intensity per unit area [*n* = 100 cells]: WT, 2.6 ± 0.5; *dnf1Δ dnf2Δ dnf3Δ*, 0.7 ± 0.2; Figure 8A, left, top). Immunoblotting demonstrated that this difference in PM decoration by Mss4-GFP was not due to any difference in expression

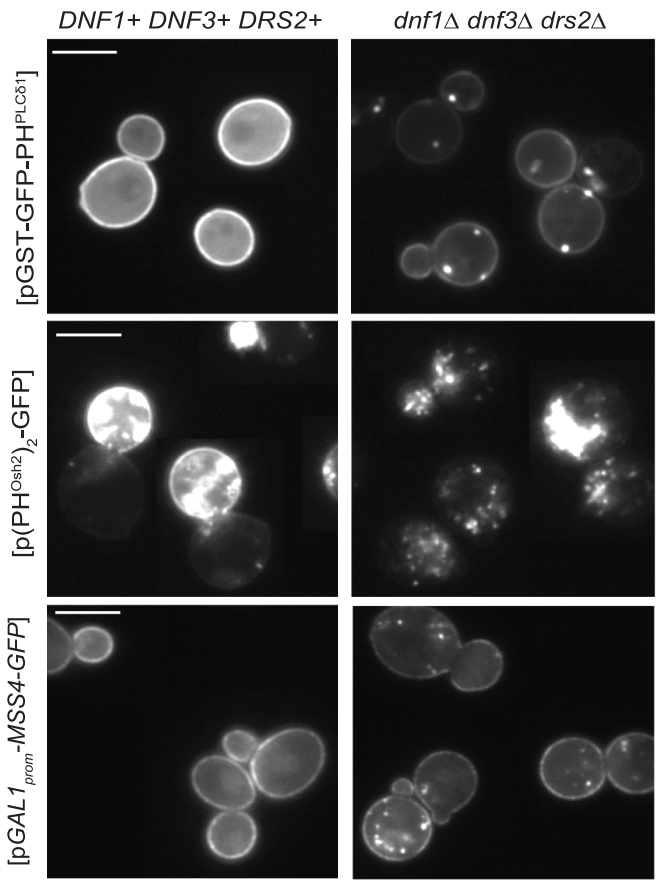

FIGURE 9: Phosphoinositide distribution is markedly perturbed in *dnf1Δ dnf3Δ drs2Δ* cells. *URA3*-marked plasmids expressing under the *GAL1* promoter either GST-GFP-PH$^{PLC\delta1}$ (top), $(PH^{Osh2})_2$-GFP (middle), or Mss4-GFP (bottom) were introduced into wild-type cells (BY4741) or an otherwise isogenic *dnf1Δ dnf3Δ drs2Δ* (ZHY708) triple mutant, and the resulting transformants were grown to mid–exponential phase in SCGlc-Ura, collected, resuspended in SCGal-Ura medium for 3 h, and then examined by fluorescence microscopy. Scale bar, 5 μm.

(Figure 8A, right). When Mss4-GFP was overexpressed, the PM decoration was much brighter, and some nuclear localization was observed in wild-type cells, as also observed previously (Audhya and Emr, 2003); however, in the *dnf1Δ dnf2Δ dnf3Δ* mutant, the PM decoration was increased only slightly, and a unique, internal, apparently vesicular compartment was prominent (Figure 8A, left, bottom).

If mislocalization of Mss4 and a resulting diminution of PM PtdIns(4,5)P_2 in *dnf1Δ dnf2Δ dnf3*Δ cells contributes to Ste5 instability by preventing its PM recruitment and thereby blocking an efficacious pheromone response, then ectopic overexpression from a strong promoter should ameliorate the problem. Toward this end, we overexpressed *MSS4* from the *GAL1* promoter on a multiple-copy plasmid in *dnf1Δ dnf2Δ dnf3*Δ cells in the absence and presence of overexpressed *STE5*. Overexpression of *MSS4* alone, but not a catalytically inactive mutant, Mss4(D636A) (Rao *et al.*, 1998; Kobayashi *et al.*, 2005), significantly increased (fourfold) the fraction of the population competent to form robust shmoos in response to α-factor treatment and further enhanced the effect of overproducing Ste5 in a modest but statistically significant manner, such that the frequency of cells in the population competent to respond to pheromone was now close to 90% of that of the wild-type cells carrying empty vector (Figure 8B).

As we demonstrated here, the *dnf1Δ dnf2Δ dnf3*Δ cells have lower levels of inner-leaflet PtdSer and PtdEth (Figure 6). As an independent means to determine whether lower levels of either of these glycerophospholipids might be responsible for lack of efficient Mss4 localization at the PM, we examined the distribution of Mss4-GFP in a *cho1Δ* mutant that lacks phosphatidylserine synthase and hence is unable to make PtdSer but can still make PtdEth via a salvage pathway (Henry *et al.*, 2012). Indeed, consistent with the lower level of inner-leaflet PtdSer in *dnf1Δ dnf2Δ dnf3Δ* cells being responsible for the poor PM recruitment and mislocalization of Mss4, we found that, in *cho1Δ* cells, Mss4 localized more weakly to the PM than in wild-type cells (average PM pixel intensity per unit area [n = 100 cells]: WT, 1.4 ± 0.2; *cho1Δ*, 0.74 ± 0.11) and very prominently to the same internal, apparently vesicular compartment seen in the *dnf1Δ dnf2Δ dnf3Δ* mutant (Figure 8C).

Through its generation of PtdIns(4,5)P_2, Mss4 has been implicated in the establishment of cell polarity (Orlando *et al.*, 2008; Yakir-Tamang and Gerst, 2009). Given the aberrations in Mss4 localization we observed in *dnf1Δ dnf2Δ dnf3*Δ cells, it was possible that there might be corresponding perturbation of the actin cytoskeleton. However, when fixed and stained with Alexa Fluor 488–labeled phalloidin, actin patch distribution, actin cable formation, and overall cytoskeletal organization in *dnf1Δ dnf2Δ dnf3*Δ cells appeared quite comparable to those in control cells (Supplemental Figure S8). Hence the failure of shmoo formation in *dnf1Δ dnf2Δ dnf3*Δ cells is not likely an indirect consequence of defects in the actin cytoskeleton.

Distribution of phosphoinositides is grossly aberrant in *dnf1Δ dnf3Δ drs2Δ* cells

We found that another flippase triple mutant, *dnf1Δ dnf3Δ drs2Δ*, also was defective in pheromone response (Figure 2, A and B), although not quite as severe as *dnf1Δ dnf2Δ dnf3Δ* cells.

However, *dnf1Δ dnf3Δ drs2Δ* cells did not exhibit a dramatic reduction in the total level of Ste5 present (Supplemental Figure S9), indicating a different underlying cause for their inability to respond to pheromone. Given the interplay between PM PtdIns(4,5)P_2 level and Ste5 stability and function that we uncovered in the course of analyzing the signaling defect in the *dnf1Δ dnf2Δ dnf3Δ* cells, we used the same probes to examine the distribution of PtdIns(4,5)P_2, PtdIns4P, and Mss4 in the *dnf1Δ dnf3Δ drs2Δ* cells.

The PtdIns4P that is converted to PtdIns(4,5)P_2 at the PM by the action of Mss4 can be supplied either by direct synthesis at the PM by the essential PtdIns 4-kinase Sst4 or delivered via Golgi compartment–derived secretory vesicles that contain PtdIns4P generated by the Golgi body–associated essential PtdIns 4-kinase Pik1 (Strahl and Thorner, 2007). We found that, compared with control cells, the distribution of the PtdIns(4,5)P_2-specific probe was strikingly different in the *dnf1Δ dnf3Δ drs2Δ* mutant. Although there was faint decoration of the PM, the most prominent fluorescent feature was several bright internal puncta (Figure 9, top). In the *dnf1Δ dnf3Δ drs2Δ* population, >70% of the cells exhibited such prominent dots, whereas <8% of wild-type cells had any sort of visible internal feature. Similarly, unlike in wild-type cells, where overexpressed Mss4-GFP is confined to the PM but faintly visible in the nucleus, the Mss4-GFP in *dnf1Δ dnf3Δ drs2Δ* cells was reduced at the PM and most prominent in a number of very bright internal puncta (Figure 9, bottom). We suspect that the reduction in PM-associated Mss4 and consequent dramatic reduction in PM PtdIns(4,5)P_2 could be sufficient, by themselves, to compromise the efficiency of Ste5 recruitment to the

PM and hence readily explain the signaling defect observed in *dnf1Δ dnf3Δ drs2Δ* cells.

Similarly, localization of the PtdIns4P-specific probe in *dnf1Δ dnf3Δ drs2Δ* cells was much less polarized than in the wild-type cells, markedly reduced at the PM, and mainly confined to small vesicles distributed roughly equally between mother and bud (Figure 9, middle). These findings indicate that, in *dnf1Δ dnf3Δ drs2Δ* cells, vesicle-mediated outbound lipid and protein trafficking is impaired, preventing efficient provision of phosphoinositides to the PM. Although phosphoinositides were not examined in prior work, our results are consistent with previous studies demonstrating that the lack of Drs2, or additional flippases in combination with Drs2, causes defects in secretory vesicle formation and trafficking from the Golgi structure to the PM, as well as in delivery of late and early endosomes to the Golgi (Chen *et al.*, 1999; Gall *et al.*, 2002; Sebastian *et al.*, 2012).

DISCUSSION

In yeast and other eukaryotes, PM bilayer composition undergoes continual remodeling due to insertion of secretory vesicles (Mizuno-Yamasaki *et al.*, 2012), removal of endocytic vesicles (Weinberg and Drubin, 2012), and action of dedicated transporters that catalyze ATP-dependent transfer of lipids from one leaflet to the other (Daleke, 2003; van Meer, 2011). The class 4 P-type ATPases that constitute the lipid flippase family in yeast (Daleke, 2007; Tanaka *et al.*, 2011; Lopez-Marques *et al.*, 2013) act on different glycerophospholipids in various cellular compartments (Muthusamy *et al.*, 2009; Sebastian *et al.*, 2012). It seems remarkable, therefore, that a yeast cell missing three of its five flippases can survive and manifests only modest morphological abnormalities despite rather profound dislocations in PM lipids, as documented here. However, flippase dysfunction has its consequences. As shown here, signaling in the mating pheromone response pathway is abrogated, due largely to effects on stability, recruitment, and/or function of MAPK scaffold protein Ste5.

In *dnf1Δ dnf2Δ dnf3Δ* cells, we traced the primary problem to inefficient PM recruitment of Mss4 and consequent reduction in PtdIns(4,5)P_2. Stable PM recruitment of Ste5 requires its PtdIns(4,5)P_2-specific PH domain (Garrenton *et al.*, 2006, 2010), and PM tethering spares Ste5 from degradation in the nucleus (Strickfaden *et al.*, 2007; Garrenton *et al.*, 2009). Hence lack of optimal Mss4-generated PtdIns(4,5)P_2 explains both the lower level of Ste5 and the signaling defect observed in *dnf1Δ dnf2Δ dnf3Δ* cells. Indeed, overexpression of both Mss4 and Ste5 largely ameliorated the signaling defect in these cells. Although several proteins are involved in PM localization of Stt4, including Sfk1 (Audhya and Emr, 2002), Ypp1, and Efr3 (Baird *et al.*, 2008), no such factor has yet been implicated in formation of the PM-associated puncta that contain Mss4, which are distinct from those harboring Stt4 (Audhya and Emr, 2002). If there are such proteins for Mss4, then our findings indicate that leaflet lipid composition may be important for their trafficking and delivery to the PM. In Mss4 (779 residues), the catalytic domain is located at its C-terminus (residues 376–769), whereas its N-terminal segment (1–375) contains no recognizable diagnostic folds. Hence perhaps the N-terminal region of Mss4 possesses protein–protein interaction elements and/or lipid-binding motifs or domains important for its PM interaction. There is some evidence that PM sphingolipid content influences Mss4 binding (Kobayashi *et al.*, 2005; Gallego *et al.*, 2010).

In *dnf1Δ dnf3Δ drs2Δ* cells, the previously characterized defect these cells exhibit in global trafficking and secretion from the Golgi compartment to the PM (Chen *et al.*, 1999; Gall *et al.*, 2002; Sebastian *et al.*, 2012) could explain its defective pheromone response, which was somewhat less severe than that of *dnf1Δ dnf2Δ dnf3Δ* cells. As shown here, the bulk of the PtdIns(4,5)P_2 and of its precursor (PtdIns4P) remains on internal membranes and thus is not efficiently delivered to the PM. In this regard, Pik1-generated PtdIns4P in the Golgi compartment binds to the C-terminal tail of Drs2 and stimulates its function (Natarajan *et al.*, 2009), suggesting that Drs2 may only be fully operative and hence able to optimally generate Golgi-derived transport vesicles when Golgi membranes are sufficiently enriched in PtdIns4P. Similarly, Osh4, which specifically binds PtdIns4P, facilitates exocyst complex–mediated secretory vesicle docking at sites of polarized growth at the PM (Alfaro *et al.*, 2011; Graham and Burd, 2011). Therefore the substantial defect we observed in PM PtdIns(4,5)P_2 in *dnf1Δ dnf3Δ drs2Δ* cells may be due, in large measure, to inefficient delivery of its precursor PtdIns4P, further suggesting that the PM-associated PtdIns 4-kinase Stt4 is not sufficient to perform this task in these cells.

In any event, PtdIns(4,5)P_2 mislocalization has significant consequences for the capacity of the cell to respond to pheromone. In this situation, because both its PH domain (Garrenton *et al.*, 2006; Garrenton *et al.*, 2010) and PM element (Winters *et al.*, 2005) display marked preference for interaction with PtdIns(4,5)P_2, any Ste5 that traffics from the nucleus will be recruited to the cytosolic surface of internal membranes rather than to the PM but nonetheless be spared from degradation. Consistent with this prediction, we found that, in contrast to *dnf1Δ dnf2Δ dnf3Δ* cells, the steady-state level of Ste5 in *dnf1Δ dnf3Δ drs2Δ* cells was not markedly reduced. However, because neither PtdIns(4,5)P_2 nor, consequently, Ste5 gets efficiently delivered to the PM, this scaffold protein will not encounter the other components of the pheromone-activated signaling apparatus (in particular, MAPKKKK Ste20) at a level sufficient to activate the Ste5-associated passenger proteins, especially the next enzyme (MAPKKK Ste11) in the MAPK cascade. These considerations likely explain the signaling deficiency of *dnf1Δ dnf3Δ drs2Δ* cells. Consistent with these conclusions, we found that overexpression of Ste5(P44L), an allele that enhances the PM targeting ability of the N-terminal amphipathic helix (PM motif) in Ste5, which can interact with other acidic phospholipids, like PtdSer (Winters *et al.*, 2005), unlike the PH domain of Ste5 (Wu *et al.*, 2012), rescued fully the shmoo formation defect of *dnf1Δ dnf3Δ drs2Δ* cells (unpublished data).

In wild-type cells responding to pheromone, Dnf1, Dnf2, and Dnf3, as well as the flippase-activating protein kinase Fpk1, exhibited dramatic relocalization to the shmoo tip. For Dnf1 and Dnf2, appearance at the tip was much more concentrated and sustained than that exhibited by Dnf3. In contrast to the other three flippases, Drs2 was visualized only in Golgi structures, with no difference in localization between vegetative and pheromone-treated cells. However, cells lacking Drs2 show a significant defect in protein transport from the *trans*-Golgi network and a reduction in the amount of Dnf1 at the cell surface (Chen *et al.*, 1999; Hua *et al.*, 2002). Hence Drs2 activity could indirectly influence Dnf1 function (and, likewise, Dnf2 and Dnf3).

Pheromone-evoked changes result in higher inner-leaflet PtdSer (Fairn *et al.*, 2011) and lower inner-leaflet PtdEth (Iwamoto *et al.*, 2004) at the shmoo tip. Thus, somehow, coordination among the three Fpk1-regulated flippases enhances the rate of inward PtdSer translocation at the expense of inward PtdEth movement. Consistent with this conclusion, the amount of PtdSer in the inner leaflet of the PM was highly reduced in *dnf1Δ dnf2Δ dnf3Δ* cells, as judged by the GFP-$C2^{Lact}$ probe. Our result is also in accord with a study showing no change in total PtdSer content in a *dnf1Δ dnf2Δ dnf3Δ* mutant compared with wild type, yet enhanced binding of another

PtdSer-specific probe, annexin V, to the exocellular surface of the PM in the mutant cells relative to wild type (Chen *et al.*, 2006).

Elevated inner-leaflet PtdSer enhances PM localization of Cdc42-GTP (Fairn *et al.*, 2011), and reduced inner-leaflet PtdEth compromises the action of Cdc42-specific GAPs (Saito *et al.*, 2007) and/or the Cdc42-directed GDI (Das *et al.*, 2012) that down-regulate Cdc42-GTP. Thus the membrane environment established in response to pheromone is conducive to maintaining a highly localized, PM-associated pool of Cdc42 in its active (GTP-bound) form, which, in turn, can stimulate the tip-associated formin Bni1 to generate actin cables that direct highly polarized secretion to support mating projection formation (Bidlingmaier and Snyder, 2004; Pruyne *et al.*, 2004).

In naive cells, Dnf1 and Dnf2 are localized throughout the PM perimeter, especially within daughters once cells have budded and at the bud neck and site of cell separation late in the cell cycle, whereas the majority of Dnf3 is in internal vesicles. The observed changes in localization during cell cycle progression and in response to pheromone (when the cells are arrested in G1) suggest that Dnf1, Dnf2, and Dnf3 localization and perhaps function are under control by the cell cycle machinery. In this regard, Dnf2 was identified among likely targets of Cdk1-Clb2 in an unbiased in vitro screen for novel substrates (Ubersax *et al.*, 2003). In addition, the flippase-activating protein kinase Fpk1 is itself under negative regulation by stress-induced protein kinase Ypk1 (Roelants *et al.*, 2010) and cell cycle–dependent protein kinase Gin4 (Roelants *et al.*, 2015). Whether Dnf1, Dnf2, and/or Dnf3, or Fpk1, Ypk1, or Gin4, are also under direct control of the pheromone-activated MAPK Fus3 remains important to investigate.

As shown here, PM lipid remodeling mediated by flippases is important for establishing conditions permissive for activation of the mating pheromone response machinery. Moreover, our studies revealed a previously unappreciated interplay between membrane phosphoinositide composition and the leaflet distribution of other classes of glycerophospholipids. It is possible that an adequate content of glycerophospholipids like PtdEth and PtdSer is necessary because their amino groups are positioned to serve as counterions for the negatively charged phosphate groups in the head groups of neighboring phosphoinositides (Slochower *et al.*, 2014). PtdIns4P and PtdIns(4,5)P_2 have been implicated in PM recruitment of proteins involved in the cell wall integrity pathway, such as Rho1 and some of its effectors (Levin, 2011). Hence, in addition to mating pheromone response, other specific PM-associated signaling processes may be similarly defective in flippase-deficient cells.

MATERIALS AND METHODS

Strains and growth conditions

Yeast strains used in this study are listed in Table 1 and were grown routinely at 30˚C. Yeast cells were cultivated in either standard rich (YP) or defined minimal (SC) medium (Sherman *et al.*, 1986) containing either 2% glucose (Glc), 2% raffinose and 0.2% sucrose (Raf-Suc), or 2% galactose (Gal) as the carbon source and, where necessary, supplemented with appropriate nutrients to maintain selection for plasmids. For induction of *GAL1* promoter-driven expression, cells were pregrown to mid–exponential phase in SCRaf-Suc medium, collected, and resuspended in Gal-containing medium (2% final concentration), and incubation was continued for 3 h. Standard yeast genetic techniques were performed according to Sherman *et al.* (1986). Strains YELO17 and YELO18 expressing Ste2(7K-to-R)-mCherry from the *STE2* promoter at the *STE2* locus were constructed by amplifying the STE2(7K-to-R)-mCherry-*CaURA3* cassette from genomic DNA of strain YDB119 (Ballon *et al.*, 2006) using primers Ste2-*Nde*I 5′-GGGTAAGTACATGATGAAACACA-TATGAA-GAAA-3′, and Ste2-*Eco*RI, TTGTAGAGCATTCATCACCATCT-TAAGCGC-3′. The resulting product was introduced by DNA-mediated transformation into BY4741 and *dnf1*Δ *dnf2*Δ *dnf3*Δ cells selecting for Ura$^+$ clones. Successful integration at the *STE2* locus was verified by colony PCR (Ward, 1992). Integration of the *FUS-1$_{prom}$-lacZ* reporter gene was accomplished by linearizing pSB286 (Trueheart *et al.*, 1987) with *Sph*I, followed by selection for Ura$^+$ transformants, which were then confirmed by colony PCR.

Plasmids and recombinant DNA methods

Plasmids used in this study are listed in Table 2. Plasmids were constructed using standard procedures (Sambrook *et al.*, 1989) in *Escherichia coli* strain DH5α. Fidelity of all constructs was verified by nucleotide sequence analysis. Plasmid pRB2 (p*GAL-MSS4*-GFP) was constructed using in vivo gap repair (Kitazono, 2009). The *MSS4*-GFP sequence was amplified by PCR from genomic DNA of a yeast strain containing a copy of *MSS4-GFP* integrated at the *MSS4* locus (Audhya and Emr, 2003) using synthetic oligonucleotide primers (Mss4-1, 5′-TACCTCTATACTTTAACGTCAAGGAGAAAA-AACCCCATGTCAGTCTTGCGATCACCACCTCCT-3′, and Mss4-2, 5′-ATGGGTACCCTACCTACTTGATATGTTACTGGTGGCGCCAC-CGCCGGCGAGATCTTGATC-3′). The resulting product and *URA3*-marked plasmid pRS316-*GAL1,10*, which had been digested with *Bam*HI and *Spe*I restriction enzymes, were introduced by DNA-mediated transformation (Pham *et al.*, 2011) into BY4741, and Ura$^+$ transformants were selected on SCGlc-Ura medium. Candidate clones were extracted, plasmid DNA was recovered in *E. coli*, and presence of the desired insert was assessed by agarose gel electrophoresis and confirmed by nucleotide sequence analysis.

A catalytically defective ("kinase-dead" [KD]) allele, p*GAL1-Mss4(D636A)-GFP* (pES20), was constructed via site-directed mutagenesis using p*GAL1-Mss4-GFP* (pES4) as the template, a pair of phosphorylated synthetic oligonucleotide primers (5′-TTATTCC-TTGTTAATTTGCATT-CATGACAT-3′ and 5′-GCCATTGTATTCAA-TTTAGCAAGCAATTC-3′), and a single-step plasmid amplification method employing Phusion polymerase (Zhang *et al*. 2009), and the resulting construct was confirmed by direct nucleotide sequencing using a reverse synthetic oligonucleotide primer starting 120 base pairs after the GFP start codon (5′-TAAGTTTTCCGTATGTTG-ACTC-3′).

Preparation of cell extracts

Preparation of yeast cell extracts by rapid alkaline lysis followed by trichloroacetic acid (TCA) precipitation was performed as described previously (Westfall *et al.*, 2008). To extract flippases efficiently from yeast cells, a few modifications were applied. Briefly, cells from samples (3 ml) of mid–exponential–phase cultures were collected and stored at –80°C overnight, and the resulting pellets were resuspended in water (500 µl final volume) and incubated on ice for 10 min with 50 µl of 1.85 M NaOH and 2% β-mercaptoethanol. After this alkaline lysis, protein was precipitated by addition of 50 µl of 50% TCA and, after incubation for 15 min on ice, collected by centrifugation at maximum speed for 5 min at room temperature in a microfuge. The resulting pellets were resuspended in urea-SDS buffer (8 M urea, 5% SDS, 0.1 mM EDTA, 0.1% bromophenol blue, 100 mM dithiothreitol, 200 mM Tris-HCl, pH 6.8), typically 60 µl/1 A_{600nm} at time of harvest, heated for 10 min at 37°C, and clarified by centrifugation at maximum speed for 2 min in a microfuge to remove any insoluble debris, and samples of the resulting supernatant solution were stored at –20°C before further analysis.

Strain	Genotype or description	Reference or source
BY4741	*MATa his3Δ1 leu2Δ0 met15Δ0 ura3Δ0*	Brachmann *et al.* (1998)
ZHY708	BY4741 *drs2Δ::LEU2 dnf1Δ::KanMX4 dnf3Δ::KanMX4*	Hua *et al.* (2002)
PFY3272C	BY4741 *dnf1Δ::KanMX4 dnf2Δ::KanMX4 dnf3Δ::KanMX4*	Hua *et al.* (2002)
YLG32	BY4741 $FUS1_{prom}$*::FUS1-lacZ::URA*	Garrenton *et al.* (2009)
YELO4	BY4741 *drs2Δ::LEU2 dnf1Δ::KanMX4 dnf3Δ::KanMX4 FUS1*$_{prom}$*::FUS1-LacZ::URA*	This study
YELO3	BY4741 *dnf1Δ::KanMX4 dnf2Δ::KanMX4 dnf3Δ::KanMX4* $FUS1_{prom}$*::FUS1-LacZ::URA*	This study
YELO9	BY4741 *dnf1Δ::KanMX4 dnf2Δ::KanMX4*	This study
YELO10	BY4741 *dnf1Δ::KanMX4 dnf3Δ::KanMX4*	This study
YELO13	BY4741 *dnf2Δ::KanMX4 dnf3Δ::KanMX4*	This study
YELO12	BY4741 *drs2Δ::KanMX4 dnf1Δ::KanMX4*	This study
YELO11	BY4741 *drs2Δ::KanMX4 dnf3Δ::KanMX4*	This study
YELO5	BY4741 *dnf1Δ::KanMX4*	This study
YELO6	BY4741 *dnf2Δ::KanMX4*	This study
YELO7	BY4741 *dnf3Δ::KanMX4*	This study
YELO8	BY4741 *drs2Δ::LEU2*	This study
NRY921	BY4741 *DNF1*-GFP::*HISMX6*	Rockwell *et al.* (2009)
NRY923	BY4741 *DNF2*-GFP::*HISMX6*	Rockwell *et al.* (2009)
YEB1	BY4741 *DNF3*-GFP::*URA3*	This study
YEB2	BY4741 *DRS2*-mCherry::*URA3*	This study
YEB6	BY4741 *NEO1*-GFP::*URA3*	This study
YFR191	BY4741 *fpk1Δ::KanMX4*	Roelants *et al.* (2010)
YFR222	BY4741 *fpk2Δ::KanMX4*	Roelants *et al.* (2010)
YFR205	BY4741 *fpk1Δ::KanMX4 fpk2Δ::KanMX4*	Roelants *et al.* (2010)
JTY6142	BY4741 *ypk1Δ::KanMX4*	Research Genetics
YELO23	BY4741 *ste5Δ::HIS3*	This study
YELO 24	BY4741 *ste5Δ::HIS3 dnf1Δ::KanMX4 dnf2Δ::KanMX4 dnf3Δ::KanMX4*	This study
YELO38	BY4741 *cln1::HIS3 cln3::LEU2*	This study
YELO39	BY4741 *cln1::HIS3 cln3::LEU2 dnf1Δ::KanMX4 dnf2Δ::KanMX4 dnf3Δ::KanMX4*	This study
YEB3	BY4741 *DRS2*-myc13::*HIS3MX6*	This study
YEB4	BY4741 *DNF1*-myc13::*HIS3MX6*	This study
YEB5	BY4741 *DNF3*-myc13::*HIS3MX6*	This study
YEB7	BY4741 *NEO1*-myc13::*HIS3MX6*	This study
YDB119	BY4741 *SST2*-GFP::*KanMX6 STE2*(7K-to-R)-mCherry::*CaURA3*	Ballon *et al.* (2006)
YELO17	BY4741 *STE2*(7K-to-R)-mCherry::*CaURA3*	This study
YELO18	BY4741 *dnf1Δ::KanMX4 dnf2Δ::KanMX4 dnf3Δ::KanMX4* Ste2(7KtoR)-mCherry::*CaURA3*	This study
JTY6525	BY4741 *cho1Δ::KanMX4*	Open Biosystems

TABLE 1: Yeast strains used in this study.

Antibodies and immunoblotting

SDS–PAGE and immunoblotting were performed as described previously (Westfall *et al.*, 2008). Proteins resolved in SDS–polyacrylamide slab gels were transferred to nitrocellulose filter paper, incubated with the appropriate primary antibodies, and then incubated with appropriate infrared dye–conjugated secondary antibodies. The resulting filter-bound immune complexes were then visualized using an Odyssey infrared imaging system (Li-Cor Biosciences, Lincoln, NE) and v2.1 software. Primary antibodies used were polyclonal rabbit anti-Ste5 antiserum (Thomson *et al.*, 2011; gift of Kirsten Benjamin, Molecular Sciences Institute, Berkeley, CA); mouse monoclonal anti-GFP (Roche Diagnostics, Indianapolis, IN); mouse monoclonal anti-myc (mAb 9E10; Evan *et al.*, 1985); rabbit polyclonal anti-Cln2 (CLN2-9099; gift of Karl Kuchler, Medical University of Vienna, Austria); rabbit polyclonal anti-Clb2 (gift of Doug Kellogg, University of California, Santa Cruz, CA); and rabbit polyclonal anti-Pgk1 (Baum *et al.*, 1978). Secondary antibodies used were Alexa Fluor 680–conjugated goat anti-rabbit immunoglobulin (IgG; Molecular Probes, Waltham, MA) and IRDye 800–conjugated goat anti-mouse IgG (Rockland Immunochemicals, Limerick, PA). Protein amounts were quantified using ImageJ software (National Institutes of Health, Bethesda, MD) and normalized levels determined as a ratio relative to the loading control (Pgk1).

Quantification of pheromone response pathway

Routinely, to gauge the ability of a given strain to respond to pheromone, the percentage of the cells in a population that were converted to unequivocally recognizable shmoos was assessed after growing the culture to mid–exponential phase, treating it with α-factor (10 μM final concentration) for, typically, 1.5 h, and then examining samples of such cultures by microscopy. As an independent measure of the capacity of cells to respond to pheromone, we used the level of induction of an integrated pheromone-responsive reporter gene, *FUS1-lacZ* (derived from plasmid pSB286), after growing cultures to mid–exponential phase, treating them with α-factor (10 μM final concentration) for, typically, 60 min, and then quantifying the level of β-galactosidase activity present using a colorimetric substrate as described previously (Bardwell *et al.*, 1998).

Plasmid	Description	Reference or source
pSB286	*FUS1*$_{prom}$*::FUS1-LacZ*	Trueheart *et al.* (1987)
pFR150	pRC181-*TPI1*$_{prom}$*-FPK1*-GFP::*LEU2*	Roelants *et al.* (2010)
YEp352GAL	2 μm DNA ORI, *URA3*, *GAL1*$_{prom}$ vector	Benton *et al.* (1994)
pAM76	YEp352-*GAL*$_{prom}$*-YPK1-myc*	Roelants *et al.* (2002)
pJT1126	YEp352-*GAL*$_{prom}$*-ypk1(K376A)-myc*	Roelants *et al.* (2002)
pS5Kmyc	*STE5*$_{prom}$*-STE5*-myc13	Winters *et al.* (2005)
pCS52	YCpU*GAL-STE5*-GFP	Sette *et al.* (2000)
pCS7	YEp352-*GAL-STE5*(P44L)	Sette *et al.* (2000)
pCS18	YCplac111-*GAL1*$_{prom}$*-STE5*(P44L)-GFP	Sette *et al.* (2000)
pLG35	YCplac111-*GAL1*$_{prom}$*-ste5*(R407S K411S)-GFP	Garrenton *et al.* (2006)
pS5Kmyc/NLSm	Ste5$_{prom}$*-ste5*(NLSm)-myc	Winters *et al.* (2005)
pGFP-C2^{Lact}	p416-*GPD*$_{prom}$-GFP-C2^{Lact}	Addgene #22853
pG-Ste4/18	pRS316-*GAL*$_{prom}$*-STE4/STE18*	Song *et al.* (1996)
pCJ6	YEp352-*GAL1-(His)*$_6$*-myc-STE5*	Inouye *et al.* (1997)
pPP1872	pGAL- GST-GFP-PH$^{PLC\delta1}$	Garrenton *et al.* (2010)
pGFP-OSH2-PH	GFP-2X-PH^{OSH2}	Roy and Levine (2004)
pCS321	pRS416-*MSS4*$_{prom}$*-MSS4-GFP*	Audhya and Emr (2003)
pRB2	pRS316-*GAL1-MSS4-GFP*	This study
YEp351GAL	2 μm DNA ORI, *LEU2*, *GAL1*$_{prom}$ vector	Benton *et al.* (1994)
pES4	YEp351-*GAL1-MSS4-GFP*	This study
pES20	YEp351-*GAL1-mss4(D636A)-GFP*	This study
pCdc24	p415-*MET25*$_{prom}$*-GFP-8A-CDC24*	Toenjes *et al.* (1999)

TABLE 2: Plasmids used in this study.

Epifluorescence and confocal fluorescence microscopy

To visualize fusion proteins marked with GFP or mCherry, cells were grown to mid–exponential phase and viewed directly under an epifluorescence microscope (Model BH-2; Olympus America, Center Valley, PA) using a 100× objective equipped with appropriate bandpass filters (Chroma Technology, Rockingham, VT). Images were collected using either an Olympus MH-228 charge-coupled device camera (Olympus America) and processed with Magnafire SP imaging software (Optronics, Goleta, CA) or a CoolSnap MYO charge-coupled device camera (Photometrics, Tucson, AZ) and processed with Micro-Manager open source microscopy software (www.micromanager.org/). For preparation of figures, images were reproduced using Photoshop (Adobe, San Jose, CA). Quantification of the fluorescence in cells was carried out using ImageJ (Collins, 2007). For each cell, its corrected total PM fluorescence was measured by determining the pixel count within an area delineated by free-form lines drawn around the inner and outer perimeter of the PM and subtracting, as background, the pixel count of an equivalent area in an immediately adjacent cell-free portion of the field. The average PM pixel intensity per unit area is the mean of such measurements performed on at least 100 cells.

Visualization of the subcellular distribution of flippases was also performed using a spinning-disk laser confocal microscopy system (Revolution XD; Andor Technology, South Windsor, CT) comprising an inverted microscope (Nikon TE 2000), a confocal spinning disk unit (model CSU-X1™; Yokogawa Electric Corp., Newman, GA), a piezo-controlled motorized *XYZ* stage, and two charge-coupled device cameras. A PlanSApo 1.4 numerical aperture/100× objective was used with 488-nm or 561-nm laser excitation. The *z*-stacks were deconvolved using Huygens Professional software (version 3.7; Scientific Volume Imaging, Amsterdam, Netherlands). Sum projections were quantified using ImageJ. All samples were imaged in aqueous media, either growth medium, or collected by brief centrifugation and resuspended in phosphate-buffered saline (PBS).

To visualize actin organization, cultures (4.5 ml) were grown to mid–exponential phase and fixed by addition of a formaldehyde solution (670 μl of fresh 37% formaldehyde stock in 0.5 ml of potassium phosphate, pH 6.5) for 1.5 h at room temperature, and the cells were collected by brief centrifugation. After three washes with 0.5 ml of PBS and resuspension in 0.5 ml of PBS, samples (0.2 ml) were incubated in the dark with constant agitation on a roller drum for 30 min with 45 μl of a solution containing Alexa Fluor 488–phalloidin (Life Technologies, Grand Island, NY; 3.3 μM Alexa Fluor 488–phalloidin and 0.1% Triton X-100 in PBS). After three washes with 0.5 ml of PBS, the final cell pellets were resuspended in 15 μl of Fluoroshield mounting buffer (Sigma-Aldrich, St. Louis, MO) and examined by fluorescence microscopy.

ACKNOWLEDGMENTS

This work was supported by National Institutes of Health R01 Research Grant GM21841 and France-Berkeley Fund Research Grant 2012-0056 (to J.T.). We thank Todd R. Graham (Vanderbilt University School of Medicine, Nashville, TN) for the gift of a *dnf1Δ dnf2Δ dnf3Δ* strain and for many useful discussions, Kurt Toenjes (Montana State University, Bozeman, MT) for providing plasmid p415Met25-GFP8A-Cdc24, Steven E. Ruzin of the College of Natural Resources Biological Imaging Facility (University of California, Berkeley, CA) for assistance with confocal fluorescence microscopy, Robert A. Arkowitz and Vikram Ghugtyal (University of Nice, Nice, France) for their hospitality and stimulating discussions, Nathan R. Rockwell (University of California, Davis, CA; formerly of this laboratory) for several gene constructs and unpublished results, and other members of the Thorner lab for additional research reagents, helpful advice, and enthusiastic encouragement.

REFERENCES

Alfaro G, Johansen J, Dighe SA, Duamel G, Kozminski KG, Beh CT (2011). The sterol-binding protein Kes1/Osh4p is a regulator of polarized exocytosis. Traffic 12, 1521–1536.

Amon A, Tyers M, Futcher B, Nasmyth K (1993). Mechanisms that help the yeast cell cycle clock tick: G2 cyclins transcriptionally activate G2 cyclins and repress G1 cyclins. Cell 74, 993–1007.
Antonny B (2011). Mechanisms of membrane curvature sensing. Annu Rev Biochem 80, 101–123.
Audhya A, Emr SD (2002). Stt4 PI 4-kinase localizes to the plasma membrane and functions in the Pkc1-mediated MAP kinase cascade. Dev Cell 2, 593–605.
Audhya A, Emr SD (2003). Regulation of PI4,5P2 synthesis by nuclear-cytoplasmic shuttling of the Mss4 lipid kinase. EMBO J 22, 4223–4236.
Baird D, Stefan C, Audhya A, Weys S, Emr SD (2008). Assembly of the PtdIns 4-kinase Stt4 complex at the plasma membrane requires Ypp1 and Efr3. J Cell Biol 183, 1061–1074.
Ballon DR, Flanary PL, Gladue DP, Konopka JB, Dohlman HG, Thorner J (2006). DEP-domain-mediated regulation of GPCR signaling responses. Cell 126, 1079–1093.
Barbosa S, Pratte D, Schwarz H, RP, Singer-Krüger B (2010). Oligomeric Dop1p is part of the endosomal Neo1p-Ysl2p-Arl1p membrane remodeling complex. Traffic 11, 1092–1106.
Bardwell L, Cook JG, Zhu-Shimoni JX, Voora D, Thorner J (1998). Differential regulation of transcription: repression by unactivated mitogen-activated protein kinase Kss1 requires the Dig1 and Dig2 proteins. Proc Natl Acad Sci USA 95, 15400–15405.
Baum P, Thorner J, Honig L (1978). Identification of tubulin from the yeast *Saccharomyces cerevisiae*. Proc Natl Acad Sci USA 75, 4962–4966.
Benton BM, Zang JH, Thorner J (1994). A novel FK506- and rapamycin-binding protein (FPR3 gene product) in the yeast *Saccharomyces cerevisiae* is a proline rotamase localized to the nucleolus. J Cell Biol 127, 623–639.
Bertin A, McMurray MA, Thai L, Garcia G 3rd, Votin V, Grob P, Allyn T, Thorner J, Nogales E (2010). Phosphatidylinositol-4,5-bisphosphate promotes budding yeast septin filament assembly and organization. J Mol Biol 404, 711–731.
Bi E, Park HO (2012). Cell polarization and cytokinesis in budding yeast. Genetics 191, 347–387.
Bidlingmaier S, Snyder M (2004). Regulation of polarized growth initiation and termination cycles by the polarisome and Cdc42 regulators. J Cell Biol 164, 207–218.
Blumer KJ, Reneke JE, Thorner J (1988). The STE2 gene product is the ligand-binding component of the alpha-factor receptor of *Saccharomyces cerevisiae*. J Biol Chem 263, 10836–10842.
Bose I, Irazoqui JE, Moskow JJ, Bardes ES, Zyla TR, Lew DJ (2001). Assembly of scaffold-mediated complexes containing Cdc42p, the exchange factor Cdc24p, and the effector Cla4p required for cell cycle-regulated phosphorylation of Cdc24p. J Biol Chem 276, 7176–7186.
Brachmann CB, Davies A, Cost GJ, Caputo E, Li J, Hieter P, Boeke JD (1998). Designer deletion strains derived from Saccharomyces cerevisiae S288C: a useful set of strains and plasmids for PCR-mediated gene disruption and other applications. Yeast 14, 115–132.
Butty AC, Perrinjaquet N, Petit A, Jaquenoud M, Segall JE, Hofmann K, Zwahlen C, Peter M (2002). A positive feedback loop stabilizes the guanine-nucleotide exchange factor Cdc24 at sites of polarization. EMBO J 21, 1565–1576.
Catty P, de Kerchove d'Exaerde A, Goffeau A (1997). The complete inventory of the yeast Saccharomyces cerevisiae P-type transport ATPases. FEBS Lett 409, 325–332.
Chen CY, Ingram MF, Rosal PH, Graham TR (1999). Role for Drs2p, a P-type ATPase and potential aminophospholipid translocase, in yeast late Golgi function. J Cell Biol 147, 1223–1236.
Chen S, Wang J, Muthusamy BP, Liu K, Zare S, Andersen RJ, Graham TR (2006). Roles for the Drs2p-Cdc50p complex in protein transport and phosphatidylserine asymmetry of the yeast plasma membrane. Traffic 7, 1503–1517.
Cole GM, Stone DE, Reed SI (1990). Stoichiometry of G protein subunits affects the *Saccharomyces cerevisiae* mating pheromone signal transduction pathway. Mol Cell Biol 10, 510–517.
Collins TJ (2007). ImageJ for microscopy. Biotechniques 43(Suppl 1), 25–30.
Daleke DL (2003). Regulation of transbilayer plasma membrane phospholipid asymmetry. J Lipid Res 44, 233–242.
Daleke DL (2007). Phospholipid flippases. J Biol Chem 282, 821–825.
Das A, Slaughter BD, Unruh JR, Bradford WD, Alexander R, Rubinstein B, Li R (2012). Flippase-mediated phospholipid asymmetry promotes fast Cdc42 recycling in dynamic maintenance of cell polarity. Nat Cell Biol 14, 304–310.
Devaux PF (1991). Static and dynamic lipid asymmetry in cell membranes. Biochemistry 30, 1163–1173.
DiNitto JP, Cronin TC, Lambright DG (2003). Membrane recognition and targeting by lipid-binding domains. Sci STKE 2003, re16.11–15.
Di Paolo G, De Camilli P (2006). Phosphoinositides in cell regulation and membrane dynamics. Nature 443, 651–657.
Divito CB, Amara SG (2009). Close encounters of the oily kind: regulation of transporters by lipids. Mol Interv 9, 252–262.
Emoto K, Umeda M (2001). Membrane lipid control of cytokinesis. Cell Struct Funct 26, 659–665.
Evan GI, Lewis GK, Ramsay G, Bishop JM (1985). Isolation of monoclonal antibodies specific for human c-myc proto-oncogene product. Mol Cell Biol 5, 3610–3616.
Fadeel B, Xue D (2009). The ins and outs of phospholipid asymmetry in the plasma membrane: roles in health and disease. Crit Rev Biochem Mol Biol 44, 264–277.
Fairn GD, Hermansson M, Somerharju P, Grinstein S (2011). Phosphatidylserine is polarized and required for proper Cdc42 localization and for development of cell polarity. Nat Cell Biol 13, 1424–1430.
Folmer DE, RP E, Paulusma CC (2009). P4 ATPases—lipid flippases and their role in disease. Biochim Biophys Acta 1791, 628–635.
Gall WE, Geething NC, Hua Z, Ingram MF, Liu K, Chen SI, Graham TR (2002). Drs2p-dependent formation of exocytic clathrin-coated vesicles *in vivo*. Curr Biol 12, 1623–1627.
Gallego O, Betts MJ, Gvozdenovic-Jeremic J, Maeda K, Matetzki C, Aguilar-Gurrieri C, Beltran-Alvarez P, Bonn S, Fernandez-Tornero C, Jensen LJ, *et al*. (2010). A systematic screen for protein-lipid interactions in Saccharomyces cerevisiae. Mol Syst Biol 6, 430.
Garrenton LS, Braunwarth A, Irniger S, Hurt E, Kunzler M, Thorner J (2009). Nucleus-specific and cell cycle-regulated degradation of mitogen-activated protein kinase scaffold protein Ste5 contributes to the control of signaling competence. Mol Cell Biol 29, 582–601.
Garrenton LS, Stefan CJ, McMurray MA, Emr SD, Thorner J (2010). Pheromone-induced anisotropy in yeast plasma membrane phosphatidylinositol-4,5-*bis*phosphate distribution is required for MAPK signaling. Proc Natl Acad Sci USA 107, 11805–11810.
Garrenton LS, Young SL, Thorner J (2006). Function of the MAPK scaffold protein, Ste5, requires a cryptic PH domain. Genes Dev 20, 1946–1958.
Gordesky M (1973). The asymmetric arrangement of phospholipids in the human erythrocyte membrane. Biochem Biophys Res Commun 50, 1027–1031.
Graham TR, Burd CG (2011). Coordination of Golgi functions by phosphatidylinositol 4-kinases. Trends Cell Biol 21, 113–121.
Groves JT, Kuriyan J (2010). Molecular mechanisms in signal transduction at the membrane. Nat Struct Mol Biol 17, 659–665.
Gulli MP, Peter M (2001). Temporal and spatial regulation of Rho-type guanine-nucleotide exchange factors: the yeast perspective. Genes Dev 15, 365–379.
Ha TS, Xia R, Zhang H, Jin X, Smith DP (2014). Lipid flippase modulates olfactory receptor expression and odorant sensitivity in Drosophila. Proc Natl Acad Sci USA 111, 7831–7836.
Hachiro T, Yamamoto T, Nakano K, Tanaka K (2013). Phospholipid flippases Lem3p-Dnf1p and Lem3p-Dnf2p are involved in the sorting of the tryptophan permease Tat2p in yeast. J Biol Chem 288, 3594–3608.
Hanamatsu H, Fujimura-Kamada K, Yamamoto T, Furuta N, Tanaka K (2014). Interaction of the phospholipid flippase Drs2p with the F-box protein Rcy1p plays an important role in early endosome to trans-Golgi network vesicle transport in yeast. J Biochem 155, 51–62.
Harkewicz R, Dennis EA (2011). Applications of mass spectrometry to lipids and membranes. Annu Rev Biochem 80, 301–325.
Henry SA, Kohlwein SD, Carman GM (2012). Metabolism and regulation of glycerolipids in the yeast *Saccharomyces cerevisiae*. Genetics 190, 317–349.
Heo WD, Inoue T, Park WS, Kim ML, Park BO, Wandless TJ, Meyer T (2006). PI(3,4,5)P3 and PI(4,5)P2 lipids target proteins with polybasic clusters to the plasma membrane. Science 314, 1458–1461.
Howell AS, Lew DJ (2012). Morphogenesis and the cell cycle. Genetics 190, 51–77.
Hua Z, Fatheddin P, Graham TR (2002). An essential subfamily of Drs2p-related P-type ATPases is required for protein trafficking between Golgi complex and endosomal/vacuolar system. Mol Biol Cell 13, 3162–3177.
Hurley JH (2006). Membrane-binding domains. Biochim Biophys Acta 1761, 805–811.
Inouye C, Dhillon N, Thorner J (1997). Ste5 RING-H2 domain: role in Ste4-promoted oligomerization for yeast pheromone signaling. Science 278, 103–106.

Iwamoto K, Kobayashi S, Fukuda R, Umeda M, Kobayashi T, Ohta A (2004). Local exposure of phosphatidylethanolamine on the yeast plasma membrane is implicated in cell polarity. Genes Cells 9, 891–903.
Kapus A, Janmey P (2013). Plasma membrane-cortical cytoskeleton interactions: a cell biology approach with biophysical considerations. Compr Physiol 3, 1231–1281.
Kato U, Emoto K, Fredriksson C, Nakamura H, Ohta A, Kobayashi T, Murakami-Murofushi K, Kobayashi T, Umeda M (2002). A novel membrane protein, Ros3p, is required for phospholipid translocation across the plasma membrane in *Saccharomyces cerevisiae*. J Biol Chem 277, 37855–37862.
Kitazono AA (2009). Improved gap-repair cloning method that uses oligonucleotides to target cognate sequences. Yeast 26, 497–505.
Kobayashi T, Takematsu H, Yamaji T, Hiramoto S, Kozutsumi Y (2005). Disturbance of sphingolipid biosynthesis abrogates the signaling of Mss4, phosphatidylinositol-4-phosphate 5-kinase, in yeast. J Biol Chem 280, 18087–18094.
Kozlov MM, Campelo F, Liska N, Chernomordik LV, Marrink SJ, McMahon HT (2014). Mechanisms shaping cell membranes. Curr Opin Cell Biol 29C, 53–60.
Künzler M, Trueheart J, Sette C, Hurt E, Thorner J (2001). Mutations in the *YRB1* gene encoding yeast Ran-binding-protein-1 that impair nucleocytoplasmic transport and suppress yeast mating defects. Genetics 157, 1089–1105.
Levin DE (2011). Regulation of cell wall biogenesis in *Saccharomyces cerevisiae*: the cell wall integrity signaling pathway. Genetics 189, 1145–1175.
Lingwood D, Simons K (2010). Lipid rafts as a membrane-organizing principle. Science 327, 46–50.
López-Marqués RL, Holthuis JC, Pomorski TG (2011). Pumping lipids with P4-ATPases. Biol Chem 392, 67–76.
Lopez-Marques RL, Theorin L, Palmgren MG, Pomorski TG (2013). P4-ATPases: lipid flippases in cell membranes. Pflugers Arch 466, 1227–1240.
Luo J, Matsuo Y, Gulis G, Hinz H, Patton-Vogt J, Marcus S (2009). Phosphatidylethanolamine is required for normal cell morphology and cytokinesis in the fission yeast *Schizosaccharomyces pombe*. Eukaryot Cell 8, 790–799.
Madden K, Snyder M (1998). Cell polarity and morphogenesis in budding yeast. Annu Rev Microbiol 52, 687–744.
Mahanty SK, Wang Y, Farley FW, Elion EA (1999). Nuclear shuttling of yeast scaffold Ste5 is required for its recruitment to the plasma membrane and activation of the mating MAPK cascade. Cell 98, 501–512.
Merlini L, Dudin O, Martin SG (2013). Mate and fuse: how yeast cells do it. Open Biol 3, 130008.
Misu K, Fujimura-Kamada K, Ueda T, Nakano A, Katoh H, Tanaka K (2003). Cdc50p, a conserved endosomal membrane protein, controls polarized growth in *Saccharomyces cerevisiae*. Mol Biol Cell 14, 730–747.
Mizuno-Yamasaki E, Rivera-Molina F, Novick P (2012). GTPase networks in membrane traffic. Annu Rev Biochem 81, 637–659.
Moravcevic K, Oxley CL, Lemmon MA (2012). Conditional peripheral membrane proteins: facing up to limited specificity. Structure 20, 15–27.
Muthusamy BP, Natarajan P, Zhou X, Graham TR (2009). Linking phospholipid flippases to vesicle-mediated protein transport. Biochim Biophys Acta 1791, 612–619.
Nakano K, Yamamoto T, Kishimoto T, Noji T, Tanaka K (2008). Protein kinases Fpk1p and Fpk2p are novel regulators of phospholipid asymmetry. Mol Biol Cell 19, 1783–1797.
Natarajan P, Liu K, Patil DV, Sciorra VA, Jackson CL, Graham TR (2009). Regulation of a Golgi flippase by phosphoinositides and an ArfGEF. Nat Cell Biol 11, 1421–1426.
Natarajan P, Wang J, Hua Z, Graham TR (2004). Drs2p-coupled aminophospholipid translocase activity in yeast Golgi membranes and relationship to in vivo function. Proc Natl Acad Sci USA 101, 10614–10619.
Noji T, Yamamoto T, Saito K, Fujimura-Kamada K, Kondo S, Tanaka K (2006). Mutational analysis of the Lem3p-Dnf1p putative phospholipid-translocating P-type ATPase reveals novel regulatory roles for Lem3p and a carboxyl-terminal region of Dnf1p independent of the phospholipid-translocating activity of Dnf1p in yeast. Biochem Biophys Res Commun 344, 323–331.
Orlando K, Zhang J, Zhang X, Yue P, Chiang T, Bi W, Guo W (2008). Regulation of Gic2 localization and function by phosphatidylinositol 4,5-bisphosphate during the establishment of cell polarity in budding yeast. J Biol Chem 283, 14205–14212.
Pham TA, Kawai S, Murata K (2011). Visualization of the synergistic effect of lithium acetate and single-stranded carrier DNA on *Saccharomyces cerevisiae* transformation. Curr Genet 57, 233–239.
Platta HW, Stenmark H (2011). Endocytosis and signaling. Curr Opin Cell Biol 23, 393–403.
Pomorski T, Lombardi R, Riezman H, Devaux PF, van Meer G, Holthuis JC (2003). Drs2p-related P-type ATPases Dnf1p and Dnf2p are required for phospholipid translocation across the yeast plasma membrane and serve a role in endocytosis. Mol Biol Cell 14, 1240–1254.
Prezant TR, Chaltraw WEJ, Fischel-Ghodsian N (1996). Identification of an overexpressed yeast gene which prevents aminoglycoside toxicity. Microbiology 142, 3407–3414.
Pruyne D, Gao L, Bi E, Bretscher A (2004). Stable and dynamic axes of polarity use distinct formin isoforms in budding yeast. Mol Biol Cell 15, 4971–4989.
Pryciak PM, Huntress FA (1998). Membrane recruitment of the kinase cascade scaffold protein Ste5 by the Gbeta/gamma complex underlies activation of the yeast pheromone response pathway. Genes Dev 12, 2684–2697.
Rao VD, Misra S, Boronenkov IV, Anderson RA, Hurley JH (1998). Structure of type II beta phosphatidylinositol phosphate kinase: a protein kinase fold flattened for interfacial phosphorylation. Cell 94, 829–839.
Rockwell NC, Wolfger H, Kuchler K, Thorner J (2009). ABC transporter Pdr10 regulates the membrane microenvironment of Pdr12 in *Saccharomyces cerevisiae*. J Membr Biol 229, 27–52.
Roelants FM, Baltz AG, Trott AE, Fereres S, Thorner J (2010). A protein kinase network regulates the function of aminophospholipid flippases. Proc Natl Acad Sci USA 107, 34–39.
Roelants FM, Breslow DK, Muir A, Weissman JS, Thorner J (2011). Protein kinase Ypk1 phosphorylates regulatory proteins Orm1 and Orm2 to control sphingolipid homeostasis in *Saccharomyces cerevisiae*. Proc Natl Acad Sci USA 108, 19222–19227.
Roelants FM, Su BM, von Wulffen J, Ramachandran S, Sartorel E, Trott AE, Thorner J (2015). Protein kinase Gin4 negatively regulates flippase function and controls plasma membrane asymmetry. J Cell Biol (*in press*).
Roelants FM, Torrance PD, Bezman N, Thorner J (2002). Pkh1 and Pkh2 differentially phosphorylate and activate Ypk1 and Ykr2 and define protein kinase modules required for maintenance of cell wall integrity. Mol Biol Cell 13, 3005–3028.
Roelants FM, Torrance PD, Thorner J (2004). Differential roles of PDK1- and PDK2-phosphorylation sites in the yeast AGC kinases Ypk1, Pkc1 and Sch9. Microbiology 150, 3289–3304.
Roy A, Levine TP (2004). Multiple pools of phosphatidylinositol 4-phosphate detected using the pleckstrin homology domain of Osh2p. J Biol Chem 279, 44683–44689.
Saito K, Fujimura-Kamada K, Furuta N, Kato U, Umeda M, Tanaka K (2004). Cdc50p, a protein required for polarized growth, associates with the Drs2p P-type ATPase implicated in phospholipid translocation in *Saccharomyces cerevisiae*. Mol Biol Cell 15, 3418–3432.
Saito K, Fujimura-Kamada K, Hanamatsu H, Kato U, Umeda M, Kozminski KG, Tanaka K (2007). Transbilayer phospholipid flipping regulates Cdc42p signaling during polarized cell growth via Rga GTPase-activating proteins. Dev Cell 13, 743–751.
Sambrook J, Fritsch EF, Maniatis T (1989). Molecular Cloning: A Laboratory Manual, 2nd ed., Cold Spring Harbor, NY: Cold Spring Harbor Laboratory Press.
Sebastian TT, Baldridge RD, Xu P, Graham TR (2012). Phospholipid flippases: building asymmetric membranes and transport vesicles. Biochim Biophys Acta 1821, 1068–1077.
Segall JE (1993). Polarization of yeast cells in spatial gradients of alpha mating factor. Proc Natl Acad Sci USA 90, 8332–8336.
Sette C, Inouye CJ, Stroschein SL, Iaquinta PJ, Thorner J (2000). Mutational analysis suggests that activation of the yeast pheromone response mitogen-activated protein kinase pathway involves conformational changes in the Ste5 scaffold protein. Mol Biol Cell 11, 4033–4049.
Shaner NC, Campbell RE, Steinbach PA, Giepmans BN, Palmer AE, Tsien RY (2004). Improved monomeric red, orange and yellow fluorescent proteins derived from Discosoma sp. red fluorescent protein. Nat Biotechnol 22, 1567–1572.
Shao C, Novakovic VA, Head JF, Seaton BA, Gilbert GE (2008). Crystal structure of lactadherin C2 domain at 1.7A resolution with mutational and computational analyses of its membrane-binding motif. J Biol Chem 283, 7230–7241.
Sherman F, Fink GR, Hicks JB (1986). Laboratory Course Manual for Methods in Yeast Genetics, Cold Spring Harbor, NY: Cold Spring Harbor Laboratory Press.
Shewan A, Eastburn DJ, Mostov K (2011). Phosphoinositides in cell architecture. Cold Spring Harb Perspect Biol 3, a004796.

Slochower DR, Wang YH, Tourdot RW, Radhakrishnan R, Janmey PA (2014). Counterion-mediated pattern formation in membranes containing anionic lipids. Adv Colloid Interface Sci 208, 177–188.
Song J, Hirschman J, Gunn K, Dohlman HG (1996). Regulation of membrane and subunit interactions by N-myristoylation of a G protein alpha subunit in yeast. J Biol Chem 271, 20273–20283.
Stahelin RV, Scott JL, Frick CT (2014). Cellular and molecular interactions of phosphoinositides and peripheral proteins. Chem Phys Lipids 182, 3–18.
Stauffer TP, Ahn S, Meyer T (1998). Receptor-induced transient reduction in plasma membrane PtdIns(4,5)P2 concentration monitored in living cells. Curr Biol 8, 343–346.
Strahl T, Thorner J (2007). Synthesis and function of membrane phosphoinositides in budding yeast *Saccharomyces cerevisiae*. Biochim Biophys Acta 1771, 353–404.
Strickfaden SC, Winters MJ, Ben-Ari G, Lamson RE, Tyers M, Pryciak PM (2007). A mechanism for cell-cycle regulation of MAP kinase signaling in a yeast differentiation pathway. Cell 128, 519–531.
Sun Y, Drubin DG (2012). The functions of anionic phospholipids during clathrin-mediated endocytosis site initiation and vesicle formation. J Cell Sci 125, 6157–6165.
Szentpetery Z, Balla A, Kim YJ, Lemmon MA, Balla T (2009). Live cell imaging with protein domains capable of recognizing phosphatidylinositol 4,5-bisphosphate; a comparative study. BMC Cell Biol 10, 67.
Takahashi Y, Fujimura-Kamada K, Kondo S, Tanaka K (2011). Isolation and characterization of novel mutations in CDC50, the non-catalytic subunit of the Drs2p phospholipid flippase. J Biochem 149, 423–432.
Takahashi S, Pryciak PM (2008). Membrane localization of scaffold proteins promotes graded signaling in the yeast MAP kinase cascade. Curr Biol 18, 1184–1191.
Tanaka K, Fujimura-Kamada K, Yamamoto T (2011). Functions of phospholipid flippases. J Biochem 149, 131–143.
Thomson TM, Benjamin KR, Bush A, Love T, Pincus D, Resnekov O, Yu RC, Gordon A, Colman-Lerner A, Endy D, *et al.* (2011). Scaffold number in yeast signaling system sets tradeoff between system output and dynamic range. Proc Natl Acad Sci USA 108, 20265–20270.
Toenjes KA, Sawyer MM, Johnson DI (1999). The guanine-nucleotide-exchange factor Cdc24p is targeted to the nucleus and polarized growth sites. Curr Biol 9, 1183–1186.
Toker A (2002). Phosphoinositides and signal transduction. Cell Mol Life Sci 59, 761–779.
Trueheart J, Boeke JD, Fink GR (1987). Two genes required for cell fusion during yeast conjugation: evidence for a pheromone-induced surface protein. Mol Cell Biol 7, 2316–2328.
Tsien RY (1998). The green fluorescent protein. Annu Rev Biochem 67, 509–544.
Ubersax JA, Woodbury EL, Quang PN, Paraz M, Blethrow JD, Shah K, Shokat KM, Morgan DO (2003). Targets of the cyclin-dependent kinase Cdk1. Nature 425, 859–864.
Vance JE, Steenbergen R (2005). Metabolism and functions of phosphatidylserine. Progr Lipid Res 44, 207–234.
van der Mark VA, Elferink RP, Paulusma CC (2013). P4 ATPases: flippases in health and disease. Int J Mol Sci 14, 7897–7922.
van Meer G (2011). Dynamic transbilayer lipid asymmetry. Cold Spring Harb Perspect Biol 3, a004671.
Ward AC (1992). Rapid analysis of yeast transformants using colony-PCR. Biotechniques 13, 350.
Weinberg J, Drubin DG (2012). Clathrin-mediated endocytosis in budding yeast. Trends Cell Biol 22, 1–13.
Westfall PJ, Patterson JC, Chen RE, Thorner J (2008). Stress resistance and signal fidelity independent of nuclear MAPK function. Proc Natl Acad Sci USA 105, 12212–12217.
Whiteway M, Hougan L, Thomas DY, Biol MC (1990). Overexpression of the *STE4* gene leads to mating response in haploid *Saccharomyces cerevisiae*. Mol Cell Biol 10, 217–222.
Wicky S, Schwarz H, Singer-Krüger B (2004). Molecular interactions of yeast Neo1p, an essential member of the Drs2 family of aminophospholipid translocases, and its role in membrane trafficking within the endomembrane system. Mol Cell Biol 24, 7402–7418.
Winters MJ, Lamson RE, Nakanishi H, Neiman AM, Pryciak PM (2005). A membrane binding domain in the ste5 scaffold synergizes with gbetagamma binding to control localization and signaling in pheromone response. Mol Cell 20, 21–32.
Wu HJ, Henzie J, Lin WC, Rhodes C, Li Z, Sartorel E, Thorner J, Yang P, Groves JT (2012). Membrane-protein binding measured with solution-phase plasmonic nanocube sensors. Nat Methods 9, 1189–1191.
Yakir-Tamang L, Gerst JE (2009). A phosphatidylinositol-transfer protein and phosphatidylinositol-4-phosphate 5-kinase control Cdc42 to regulate the actin cytoskeleton and secretory pathway in yeast. Mol Biol Cell 20, 3583–3597.
Ye H, Li B, Subramanian V, Choi BH, Liang Y, Harikishore A, Chakraborty G, K B, HS Y (2013). NMR solution structure of C2 domain of MFG-E8 and insights into its molecular recognition with phosphatidylserine. Biochim Biophys Acta 1828, 1083–1093.
Yeung T, Gilbert GE, Shi J, Silvius J, Kapus A, Grinstein S (2008). Membrane phosphatidylserine regulates surface charge and protein localization. Science 319, 210–213.
Zhang BZ, Zhang X, An XP, Ran DL, Zhou YS, Lu J, Tong YG (2009). An easy-to-use site-directed mutagenesis method with a designed restriction site for convenient and reliable mutant screening. J Zhejiang Univ Sci B 10, 479–482.
Zhao M (2011). Lantibiotics as probes for phosphatidylethanolamine. Amino Acids 41, 1071–1079.